

Time evolution of the local density of states of strongly correlated fermions coupled to a nanoprobe

T. Blum,¹ R.M. Noack,¹ and S.R. Manmana²

¹*Fachbereich Physik, Philipps-Universität Marburg, 35032 Marburg, Germany*

²*Institut für Theoretische Physik, Georg-August-Universität Göttingen, 37077 Göttingen, Germany*

(Dated: July 23, 2024)

We study the time evolution of a one-dimensional system of strongly correlated electrons (a ‘sample’) that is suddenly coupled to a smaller, initially empty system (a ‘nanoprobe’), which can subsequently move along the system. Our purpose here is to study the role of interactions in this model system when it is far from equilibrium. We therefore take both the sample and the nanoprobe to be described by a Hubbard model with on-site repulsive interactions and nearest-neighbor hopping. We compute the behavior of the local particle density and the local density of states (LDOS) as a function of time using time-dependent matrix product states at quarter and at half filling, fillings at which the chain realizes a Luttinger liquid or a Mott insulator, respectively. This allows us to study in detail the oscillation of the particles between the sample and the nanoprobe. While, for noninteracting systems, the LDOS is time-independent, in the presence of interactions, the backflow of electrons to the sample will lead to nontrivial dynamics in the LDOS. In particular, studying the time-dependent LDOS allows us to study how the Mott gap closes locally and how this melting of the Mott insulator propagates through the system in time after such a local perturbation—a behavior that we envisage can be investigated in future experiments on ultrashort time scales or on optical lattices using microscopy setups.

I. INTRODUCTION

One very common and interesting scenario in physics occurs when two systems are coupled to one another starting at a particular point in time and then interact with one another in a time-dependent way. The salient physical question is how the two systems then evolve in time. When the two systems are quantum many-body systems, particularly interesting behavior can be expected.

The study of such nonequilibrium correlated systems is inspired by fundamental issues such as the nature of thermalization in closed quantum systems [1–4], the behavior found in controlled experimental investigations in cold atomic gases on optical lattices [5, 6], and by the study of material properties after a strong photo excitation, typically in the context of pump-probe experiments [7–10]. These advanced time-resolved experimental techniques make it possible to study a variety of nonequilibrium phenomena, such as the formation of transient order, light-induced phase transitions, or hidden states on ultra-short time scales (pico-

or femtoseconds) [11–24]. One such experimental approach is time- and angular resolved photo emission spectroscopy (trARPES) [25], which provides direct insights into nonequilibrium properties of spectral functions, e.g., the existence of Floquet states [26–34], which have been proposed as a means of engineering certain material properties such as topological states in periodically driven systems [31, 35, 36].

Typically, trARPES measurements are made in momentum space; in order to gain insights into the behavior of observables in real space, one would thus need to Fourier-transform the data [37]. For locally restricted excitations (e.g., ones induced by the tip of a scanning tunneling microscope (STM) [38, 39]), it can be important to investigate the evolution of spectral properties directly in position space. While STM experiments typically deal with transport properties in the linear-response regime and hence remain close to equilibrium (see, e.g., Ref. 40 for a recent review article), it is also interesting to consider such situations far away from equilibrium. Here we treat this case, computing the time evolution of the *local* density of states

(LDOS) when strongly perturbing a strongly correlated system only locally. We envisage that this quantity will be experimentally accessible in the future, also on the ultrashort time scales treated by us here.

Inspired by these considerations, we ask the question of what happens when a small, initially empty, test system (in the following referred to as a ‘nanoprobe’ or ‘probe’) is brought near a sample hosting a strongly correlated state of matter. We assume a strong coupling between the sample and the nanoprobe, which also allows for electrons to flow from the probe back to the sample. This will induce a dynamics that is far from the linear-response regime, so that an equilibrium description does not apply. One important aspect is to what extent measures from linear response theory are useful to describe such a situation. We quantify this by considering in detail the properties of the LDOS computed from time-dependent single particle propagators. The behavior of the LDOS is particularly interesting for strongly correlated electrons because the time-evolved LDOS can exhibit nontrivial features induced by significant electron-electron interaction: whereas the LDOS remains time-independent after the sudden coupling for noninteracting systems (as discussed later in the paper), this is no longer true for strongly interacting systems, and the behavior of the LDOS can change significantly in the course of time.

Here we study these aspects on a ‘standard’ model for strongly correlated physics, namely, the Hubbard model in one spatial dimension [41, 42]. At finite repulsive interaction strength, this model exhibits Mott-insulating behavior [43] at half filling and is a Luttinger liquid [44] otherwise. Our setup allows us to study and compare the time evolution of the LDOS in the two qualitatively different phases by tuning the initial filling.

The remainder of the paper is organized as follows: In Sec. II, we describe the model, the quantities that we study, and the methods that

we use. In particular, in Sec. II A, we describe the setup of our model system and the time-dependent coupling between sample and nanoprobe. In Sec. II B, we discuss the observables we compute, in particular the time-dependent LDOS. Section II C describes our matrix-product-state (MPS) approach to simulating the dynamics of the system as well as the exact solution for the $U = 0$ case. In Sec. III we present our results for both the stationary and the moving nanoprobe. Finally, we discuss and summarize our findings in Sec. IV. In addition, App. A describes estimates of the accuracy of our calculations by comparing to the exact results at $U = 0$, and App. B contains additional results for a higher nanoprobe velocity, $v = 1$.

II. MODEL, OBSERVABLES, AND METHODS

A. Model

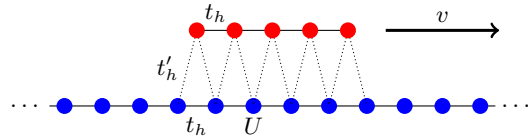


FIG. 1. Schematic depiction of the setup. Blue sites are in the sample and red sites in the nanoprobe. The tunneling strength t_h and the onsite Hubbard U have each the same values in the sample and the probe, respectively. The tunneling strength t'_h between sample and nanoprobe is finite only at times $t > 0$. The nanoprobe can move to the right with a constant speed $v \geq 0$ relative to the sample.

We study the one-dimensional Hubbard model [41, 42], which, at time $t = 0$, is suddenly coupled to a set of initially empty interacting sites, which represent the nanoprobe, as depicted in Fig. 1. This system is modeled by the Hamiltonian

$$\begin{aligned}
H = & -t_h \sum_{k \in \{\text{sample, probe}\}} \sum_{\sigma} \left(c_{k,\sigma}^{\dagger} c_{k+1,\sigma} + c_{k+1,\sigma}^{\dagger} c_{k,\sigma} \right) + U \sum_{k \in \{\text{sample, probe}\}} n_{k,\uparrow} n_{k,\downarrow} \\
& - t'_h \sum_{i \in \text{sample}} \sum_{j \in \text{probe}} \sum_{\sigma} w(t, i, j) \left(c_{i,\sigma}^{\dagger} c_{j,\sigma} + c_{j,\sigma}^{\dagger} c_{i,\sigma} \right),
\end{aligned} \tag{1}$$

with

$$w(t, i, j) = \Theta(t) \left[\Theta \left(vt - i + j + \frac{L-l}{2} + 1 \right) - \Theta \left(vt - i + j + \frac{L-l}{2} - 1 \right) \right], \tag{2}$$

where $\Theta(x)$ is the Heaviside function, t the time, and we take the lattice constant to be 1. We designate the number of sites in the sample L , the number of sites in the nanoprobe l with index $i \in \{1, \dots, L\}$ in the sample and $j \in \{1, \dots, l\}$ in the probe and work in the canonical ensemble with a fixed number of particles N . In Hamiltonian (1), we assume open boundary conditions (OBC). The function $w(t, i, j)$ causes each site of the nanoprobe to be coupled to the two nearest sites in the sample only for all times $t > 0$. The operator $c_{i,\sigma}^{(\dagger)}$ represents the annihilation (creation) operator for an electron with spin σ on lattice site i , and $n_{i,\sigma} = c_{i,\sigma}^{\dagger} c_{i,\sigma}$ is the electron density for spin σ at site i . Here t_h is the hopping amplitude inside the sample and inside the nanoprobe; in the following, we work in units in which $t_h \equiv 1$ and take $\hbar \equiv 1$. The coupling t'_h is the hopping amplitude between sample and probe. The parameter $U \geq 0$ denotes the strength of the repulsive on-site interaction between the electrons, which we assume to be the same in the sample and in the probe. If not stated explicitly otherwise, we take $U = 4$, a value corresponding to the bandwidth of the sample at $U = 0$. In the following, we will also study the situation in which the nanoprobe moves with a constant speed v over the sample. For speeds $v > 0$, the hoppings between the nanoprobe and the sample are adjusted in time according to the function $w(t, i, j)$ which leads to a sequence of quantum quenches.

B. Observables

1. Local particle density $\langle n_i \rangle$

In all cases, we compute the time evolution of the local particle density $n_i(t) \equiv \langle \psi(t) | n_i | \psi(t) \rangle$. Due to the strong tunneling between sample and nanoprobe, we expect the backflow of electrons to lead to nontrivial behavior in this quantity. Furthermore, coupling the nanoprobe to the sample is a local quench, so that we expect that a perturbation will propagate through the sample, leading to a light-cone-like signature in $n_i(t)$. Note that for the Mott insulator at half filling, the flow of electrons from the sample to the nanoprobe will move the sample away from half filling, so that it should then lose the properties of a Mott insulator in the course of time. In particular, this should affect the Mott gap, which is visible in the LDOS.

2. Time-dependent local density of states

We calculate the time evolution of the energy-resolved LDOS at position i , $D_{\sigma}(t, \omega, i)$, as the Fourier transform of the retarded two-time Green's function (see, e.g., Ref. 45 for a similar approach to computing the nonequilibrium single-particle spectral function),

$$D_{\sigma}(t, \omega, i) = \text{Re} \left[\frac{1}{\sqrt{2\pi}} \int_{-\infty}^{\infty} \Theta(\tau) d\tau W(\tau) e^{i\omega\tau} \left\langle \left\{ c_{i,\sigma}(t+\tau), c_{i,\sigma}^{\dagger}(t) \right\} \right\rangle \right], \tag{3}$$

where the operator $c_{i,\sigma}^{(\dagger)}(t)$ is the annihilation (creation) operator for an electron with spin σ at position i in the Heisenberg picture evolved with the full, time-dependent Hamiltonian $H(t)$ at time t , and $\{\cdot, \cdot\}$ denotes the usual anticommutator. Note that alternative ways of computing momentum- and energy-resolved time-dependent spectral functions that avoid carrying out a Fourier transform to frequency space do exist; see, e.g., Ref. 46. Here, however, we study the local spectral properties using the more direct definition of the LDOS based on linear response theory, Eq. (3), and compare the results to the equilibrium expectations, giving us a quantitative measure for how strongly our time-dependent LDOS deviates from the linear-response regime.

As discussed further below, we can compute the two-time Green's function up to a restricted maximal time τ_{\max} , so that it is necessary to regularize the integral either by introducing a damping term $e^{-\eta\tau}$ or to introduce a windowing function in order to avoid ringing effects caused by a sudden cut-off of the data at $\tau = \tau_{\max}$ [47]. We find here that applying the Hann window, which is defined as

$$W(\tau) = \Theta(\tau_{\max} - |\tau|) \sin^2 \left(\frac{\pi\tau}{2\tau_{\max}} + \frac{\pi}{2} \right),$$

leads to the best results.

Note that, at equilibrium (linear response theory), the time evolution of $c_{i,\sigma}^{(\dagger)}(t)$ is carried out using the Hamiltonian of the unperturbed system, so that time-translation invariance can be used to reduce the time dependence of the Green's function to one time variable. Since time-translation invariance is absent out of equilibrium (e.g., in the quench we perform here at time $t = 0$), we need to treat the full time dependence of the two-time Green's function. Here we use a relative-time representation of the retarded two-time Green's function, i.e., $\langle \{ c_{x,\uparrow}(t + \tau), c_{x,\uparrow}^\dagger(t) \} \rangle$. This has two helpful aspects: (i) we can interpret the variable t as

the waiting time after switching on the coupling between the nanoprobe and the sample and ask for the behavior of the LDOS at this waiting time. (ii) It makes the numerical evaluation of this quantity easier. This is the case because, due to the Heaviside function $\Theta(\tau)$, we only need to compute the Green's function for $\tau > 0$. Rather than this relative-time representation, one could instead use the so-called Wigner representation (see, e.g., Ref. 48), for which, however, one would also need to compute expectation values at further points in time, increasing the computational cost. According to Ref. 48, the results in both representations do not differ significantly, so that we choose to work in the relative-time representation for the sake of efficiency.

Due to the limitations of the numerical approaches, we have evaluated the integral numerically using a time step $d\tau = 0.01$ up to times $\tau_{\max} = 5$ (except that we take $\tau_{\max} = 20$ for the $U = 0$ case, which can be treated exactly). However, we discretize ω at 2000 equally spaced points between $\omega_{\min} = -10$ and $\omega_{\max} = 10$ by interpolation using zero-padding. Note that, at equilibrium, the LDOS defined in this way can be expressed as a Lehmann representation with positive weights, so that an interpretation as a spectral weight is natural. However, this is no longer possible in the nonequilibrium case, and negative weights can, in principle, appear [49]. As discussed further below, we observe negative weights only at short times, at which the system is strongly out of equilibrium, but, at later times, negative weights seem to be absent, so that an interpretation of the results in terms of spectral weights is possible. Similarly, in nonequilibrium situations, one needs to be careful about identifying the occupied and unoccupied parts of the LDOS: at equilibrium, one usually introduces the lesser and the greater parts of the LDOS, $B_\sigma^<(\omega, i)$ and $B_\sigma^>(\omega, i)$ [50], which indicate the populated and empty states on lattice site i , respectively. Out of equilibrium, one can generalize these functions as follows:

$$B_{\sigma}^{<}(t, \omega, i) = \text{Re} \left[\frac{1}{\sqrt{2\pi}} \int_0^{\tau_{\max}} d\tau W(\tau) e^{i\omega\tau} \langle c_{i,\sigma}^{\dagger}(t) c_{i,\sigma}(t+\tau) \rangle \right], \quad (4)$$

$$B_{\sigma}^{>}(t, \omega, i) = \text{Re} \left[\frac{1}{\sqrt{2\pi}} \int_0^{\tau_{\max}} d\tau W(\tau) e^{i\omega\tau} \langle c_{i,\sigma}(t+\tau) c_{i,\sigma}^{\dagger}(t) \rangle \right]. \quad (5)$$

Note that, due to the lack of a Lehmann representation, both quantities can become negative. Furthermore, linear response theory requires time-translation invariance in order to interpret these quantities as occupied or empty parts of the spectrum, respectively. Here, due to the nonequilibrium setup, we do not have this symmetry when going to negative τ , so that we can only expect these quantities to represent the occupied (empty) part of the LDOS approximately. We will come back to this interesting aspect in Sec. III A 4, where we discuss how to estimate the occupied states in $D_{\sigma}^{<}(t, \omega, i)$ at lattice site i by comparing to $\langle n_{i,\sigma} \rangle(t)$.

3. Nonequilibrium occupation energy

At equilibrium, the LDOS is obtained as

$$D_{\sigma}^{\text{eq}}(\omega, i) = \text{Re} \left[\frac{1}{\sqrt{2\pi}} \int_{-\infty}^{\infty} \Theta(\tau) d\tau W(\tau) e^{i\omega\tau} \left\langle \left\{ c_{i,\sigma}(\tau)^{H_0}, c_{i,\sigma}^{\dagger}(0)^{H_0} \right\} \right\rangle \right], \quad (6)$$

where H_0 indicates that the time evolution of the operators is carried out using the unperturbed Hamiltonian, and, due to time-translation invariance, only one time variable needs to be treated. Integrating the equilibrium LDOS $D_{\sigma}^{\text{eq}}(\omega, i)$ in energy up to the Fermi level E_F will yield the local particle density $\langle n_{i,\sigma} \rangle$, so that the LDOS below E_F can be interpreted as the occupied part. The Fermi energy E_F is hence the value of the energy of the highest populated state in the system. Similarly, at

equilibrium, one can introduce

$$B_{\sigma}^{<,\text{eq}}(\omega, i) = \text{Re} \left[\frac{1}{\sqrt{2\pi}} \int_{-\infty}^{\infty} d\tau W(\tau) e^{i\omega\tau} \left\langle c_{i,\sigma}^{\dagger}(0)^{H_0} c_{i,\sigma}(\tau)^{H_0} \right\rangle \right] \quad (7)$$

as the lesser part of the LDOS. Note that $B_{\sigma}^{<,\text{eq}}(\omega, i)$ does not have weights for energies higher than E_F , so that $\int_{-\infty}^{\infty} d\omega B_{\sigma}^{<,\text{eq}}(\omega, i) = \langle n_{i,\sigma} \rangle$. Hence, $B_{\sigma}^{<,\text{eq}}(\omega, i)$ represents the occupied part of the LDOS. Out of equilibrium, however, one needs to be more careful. A simple way to identify the populated states is to assume that only the lowest-energy parts of the nonequilibrium LDOS $D_{\sigma}(t, \omega, i)$ are occupied. Integrating $D_{\sigma}(t, \omega, i)$ at site i at fixed waiting time t up to a certain energy, which we call E_{occ} , should give the same result as $\langle n_{i,\sigma} \rangle(t)$. The value $E_{\text{occ}}(t)$ can then be interpreted as the nonequilibrium generalization of E_F . We define E_{occ} implicitly via

$$\frac{1}{C} \int_{-\infty}^{E_{\text{occ}}(t,i)} d\omega D_{\sigma}(t, \omega, i) = \langle n_{i,\sigma} \rangle(t), \quad (8)$$

with the normalization $C = \int_{-\infty}^{\infty} d\omega D_{\sigma}(t, \omega, i)$. In the following, spin-flip symmetry is present; thus, for simplicity, we only discuss the $\sigma = \uparrow$ component of both the LDOS and the particle density.

Furthermore, we can compare the expectation value for the number of particles as obtained from the energy integral $\int d\omega B_{\sigma}^{<}(t, \omega, i)$ at fixed t and i with the directly computed expectation value $\langle n_{\sigma,i} \rangle(t)$, which, in equilibrium, is identical, as discussed above. Differences from this expectation value can be considered to be a measure of how far away from equilibrium the system is. As discussed further below, significant deviations are obtained at short times

in particular, indicating strong nonequilibrium behavior, while, at later times, both quantities agree to within a few percent. The time evolution of $E_{\text{occ}}(t)$ also indicates how particles are redistributed in the course of time, in particular, for the cases in which the LDOS is changing in time due to the strong interactions in the system.

C. MPS-based methods

1. Initial state preparation and time evolution

All calculations for the interacting system have been performed at $U = 4$ using a density matrix renormalization group (DMRG) algorithm [51, 52] within the MPS framework [53, 54], which is available in the SymMps toolkit [55].

The general procedure is as follows. For $U = 4$, we calculate the ground state on a system with $L = 50$ sample lattice sites and $l = 5$ nanoprobe sites for the quarter- and half-filled samples, with $N = 26$ and $N = 50$ particles, respectively. (We take $N = 26$ rather than $N = 25$ particles for quarter filling so that the number of spin-up and spin-down particles is equal.) Initially, the nanoprobe is not yet coupled to the system, i.e., $t'_h = 0$. To ensure a state with zero occupation at time $t = 0$ in the nanoprobe, we add a small repulsive electrostatic potential $\sum_{j \in \text{probe}} \mu_j(n_{j,\uparrow} + n_{j,\downarrow})$ on these sites. We then perform a ground-state search with a maximum bond dimension of $\chi = 2500$ and a maximum discarded weight of $\delta = 10^{-14}$ with a total of 50 sweeps. This allows us to approximate the ground state of the system with an absolute error in the ground state energy of 3.0×10^{-6} in the quarter-filled case, compared to the exact value known from Bethe Ansatz [42, 56]. The absolute error in the ground-state energy in the half-filled case is even smaller, 1.7×10^{-7} .

At time $t = 0$, the electrostatic potential in the nanoprobe is then set to zero, and it is immediately coupled to the system with the full hopping strength, $t'_h = t_h$. We compute

the subsequent time evolution of the total system using the time-dependent variational principle (TDVP) in its two-site version using MPS [57, 58]. This allows us to treat systems with arbitrary coupling ranges and to adjust the bond dimension in the course of the time evolution, keeping track of the growth of entanglement with time. It is known that the TDVP can have substantial problems with product initial states. Alternatively, one could use the matrix product operator (MPO) WII time-evolution algorithm [58, 59], which does not suffer from such problems. Here we have tested both algorithms, comparing with exact diagonalization for systems with 3 particles, and we find that the errors of the TDVP for the given setup are an order of magnitude smaller than those of the MPO WII algorithm. The MPO WII has a maximum absolute error of $\approx 4 \times 10^{-4}$ in $n_i(t)$ for this test case, whereas the TDVP algorithm reaches a maximum error of $\approx 5 \times 10^{-5}$. In addition, in App. A, we compare the time evolution of the half-filled case at $U = 0$ as obtained from MPS with that of the exact solution (see Sec. II C 3). As shown there, the absolute errors grow in time. For $v = 0$, we find that the absolute errors in $\langle n_{i,\sigma} \rangle(t)$ are $\lesssim 0.05$ at later times, and the absolute errors in the LDOS are $\lesssim 0.015$, while for the moving probe the errors in the LDOS are even smaller, although the absolute errors in $\langle n_{i,\sigma} \rangle(t)$ can be as high as ~ 0.1 at isolated points. Hence, we believe that our results are sufficiently accurate to extract the essential physical behavior.

We set the threshold for the discarded weight during the time evolution to $\delta = 10^{-10}$ and the maximum bond dimension to $\chi_{\text{max}} = 2500$. The time step size is $\delta t = 0.01$ for all results presented. As discussed in App. A, the resulting discarded weight at later times is rather large, almost 10^{-4} ; however, due to the high computational cost, we do not further increase the bond dimension or carry out calculations to longer times.

We perform the time evolution so that, for all waiting times, the integration time is $\tau_{\text{max}} = 5$ after the waiting time (i.e., for waiting time $t = 5$, we perform the simulations up to times

$t + \tau_{\max} = 10$). In this way, all the presented results at different waiting times have the same resolution in ω .

For a finite speed $v > 0$ of the probe, the Hamiltonian is explicitly time-dependent. In principle, more accurate results can be obtained by applying more elaborate discretization schemes on the time variable, such as commutator-free exponential time (CFET) propagators [60]. However, in our case, due to the structure of the function $w(t, i, j)$ in the Hamiltonian (1), the time-dependence of H is not continuous, but comes in steps at points in time determined by the value of v . The time evolution for $v > 0$ is, therefore, realized as a sequence of quantum quenches, for which the usual methods (here the TDVP) perform well.

2. Swap operator

For the case of the moving nanoprobe, i.e., $v > 0$, the hopping terms to the sample become longer range with time, which leads to larger entanglement between the two parts of the system and hence makes the MPS description less accurate. In our case, we have only nearest-neighbor and next-nearest-neighbor hopping at time $t = 0$; it is useful to keep the hopping as short-range as possible in the course of the time evolution. We address this by introducing the swap operator (see Ref. 61 for the usage of swap operators for time-evolution algorithms),

$$P_i = \prod_{\sigma=\uparrow,\downarrow} \left[1 - \left(c_{i,\sigma}^\dagger - c_{i+1,\sigma}^\dagger \right) \left(c_{i,\sigma} - c_{i+1,\sigma} \right) \right], \quad (9)$$

which is applied at the points in time when the probe, according to the function $w(t, i, j)$, Eq. (2), couples to new sites in the sample. In this way, the site labeling is adapted so that the hopping terms for all times treated are either nearest-neighbor or next-nearest-neighbor terms, thus minimizing the entanglement growth in the course of time.

3. Solution for $U = 0$

In the noninteracting case, $U = 0$, we can solve the system exactly by diagonalizing the Hubbard Hamiltonian (1) for a single particle. In doing this, we add an additional chemical potential of $\mu = 10^8$ to the sites of the nanoprobe so that the wave-function amplitude is vanishingly small there. This ensures that the initial many-body state has zero particle density on the nanoprobe before the coupling between nanoprobe and sample is turned on at $t = 0$. This then yields the single-particle wave functions $\phi_{i,n}(0)$, where i denotes the lattice site and n refers to the n -th excited state for a single particle, with $n = 1$ being the single-particle ground state. The time-dependent state $|\psi_i(t)\rangle$ is then easily obtained by applying the time-evolution operator e^{-iHt} :

$$|\psi_i(t)\rangle = \left(\sum_{n=1}^{N_\uparrow} \phi_{i,n}(t) c_{n,\uparrow}^\dagger + \sum_{n=1}^{N_\downarrow} \phi_{i,n}(t) c_{n,\downarrow}^\dagger \right) |0\rangle,$$

where $\phi_{i,n}(t) = e^{-iHt} \phi_{i,n}(0)$ are the time-evolved single-particle states. The time-dependent LDOS $D_\sigma(t, \omega, i)$ can then be calculated via the transformation $c_{i,\uparrow}(t) = \sum_{n'} \phi_{i,n'}(t) c_{n',\uparrow}$. Note that n refers to the single-particle states for the decoupled system; n' , however, refers to the single-particle eigenstates after coupling the nanoprobe to the Hubbard chain. Inserting this expression into Eq. (3) leads to a simple expression for the two-time Green's function:

$$\left\langle \left\{ c_{i,\sigma}(t + \tau), c_{i,\sigma}^\dagger(t) \right\} \right\rangle = \sum_{n'} \phi_{i,n'}(t + \tau) \phi_{i,n'}^*(t). \quad (10)$$

This expression is independent of the number of particles in the system, as particles and holes lead to the same contribution for the LDOS in the $U = 0$ case. Furthermore, at $v = 0$, i.e., for a time-independent Hamiltonian, the LDOS of the noninteracting system is time-independent

because the dependence on t in Eq. (10) vanishes for $e^{-iH(t+\tau)} e^{iHt} = e^{-iH\tau}$. Note that Eq. (10) can be calculated accurately to arbitrarily long times, so that, in contrast to the MPS results at finite U , we can obtain much better resolution in ω .

III. RESULTS

In this section, we present representative results for the time evolution of our setup. We organize the discussion by first considering a stationary nanoprobe, i.e., one that does not move over the sample, $v = 0$, then going on to a relatively slow nanoprobe with $v = 0.55$. We have also carried out calculations at a higher velocity, $v = 1$, which are presented in App. B; we will also describe the salient aspects of the behavior relative to that of $v = 0.55$ in the main text. For all values of v , we first discuss the behavior of the noninteracting case, $U = 0$, then present results for the interacting case, taking the Hubbard interaction to have intermediate strength, $U = 4$. For all cases, we take a system with $L = 50$ sample sites with $l = 5$ initially empty probe sites and treat two values of the band filling, quarter filling with $N = 26$ particles and half filling, with $N = 50$ particles. We present the results for the time evolution of the local particle density in the sample and in the nanoprobe as well as the LDOS at three fixed positions: in the sample far away from the nanoprobe, site $i_s = 13$, in the sample directly under the nanoprobe, site $i_s = 26$, and in the center of the nanoprobe, site $i_p = 3$. All results are obtained for samples with $L = 50$ lattice sites and nanoprobe with $l = 5$ lattice sites.

A. Resting nanoprobe: $v = 0$

We first consider the case in which the nanoprobe does not move, i.e., $v = 0$. As soon as the tunneling between the system and the nanoprobe is turned on at time $t = 0$, the system evolves nontrivially in time as it undergoes a quantum quench. As the tunneling will also

be turned on at $t = 0$ for the cases of a moving nanoprobe, the $v = 0$ behavior will provide a basis for the interpretation of the moving cases. Since the nanoprobe initially holds no particles, particles will begin tunneling from the system to the nanoprobe at $t = 0$.

1. Noninteracting case $U = 0$

We start with the noninteracting case, $U = 0$. In Fig. 2(a), we display the expectation value of the local particle density $n_i(t)$ for the quarter-filled system as a color density plot plotted as a function of position and time. As can be seen in the plot, at time $t = 0$, the nanoprobe is completely empty of particles. After the tunneling to the system is turned on ($t > 0$), the particles begin to tunnel back and forth, leading to oscillations in time in the local particle density in both the nanoprobe and in the region of the system in its vicinity. These oscillations are somewhat spatially inhomogeneous both in the system and in the nanoprobe, with the strongest fluctuations of particle density occurring near the center of the nanoprobe. As time progresses, the time dependence in local particle density spreads out in time. In particular, a “light cone” that spreads out across the sample at constant speed $c \approx 1.6$, which we have estimated by roughly fitting the wave front, is evident. In Figs. 2(b)–(d), we display the LDOS $D_{\uparrow}(t, \omega, x)$ for this case at sites $i_s = 13$ and $i_s = 26$ in the sample and $i_p = 3$ in the nanoprobe. Sites $i_s = 26$ and $i_p = 3$ are directly next to each other and become directly linked by hopping terms as soon as the coupling between probe and sample is turned on. For $U = 0$ and a speed of $v = 0$, the LDOS is time-independent for all sites after the coupling is turned on. This is to be expected because the Hamiltonian is time-independent for $t > 0$ in this case, and there is no scattering between the electrons; see also the discussion in Sec. II C 3. Thus, we display the LDOS for time $t = 0$ only. For $i_s = 13$, Fig. 2(b), we observe peaks at $\omega \approx -2$ and $\omega \approx 2$, with an oscillating and non-vanishing LDOS in between the peaks.

At sample site $i_s = 26$ and probe site $i_p = 3$, which are adjacent to one another, we can see that the LDOS for both sites have peaks that are largely at the same ω positions, with only the amplitudes differing somewhat. In contrast to the LDOS for $i_s = 13$, there is a major peak at $\omega \approx -4$ for these two sites. Regarding the occupation energies, we find that $E_{\text{occ}}(t)$ is essentially time-independent on lattice site $i_s = 13$, indicating no (or only very little) redistribution of particles on the time scale considered. This is to be expected, as the light-cone-like perturbation in $n_i(t)$ reaches this position only at later times, $t > 5$, which are not shown. At site $i_s = 26$, $E_{\text{occ}}(t)$ is initially close to the equilibrium Fermi energy at site $i_s = 13$. After the nanoprobe is coupled to the sample, $E_{\text{occ}}(t)$ begins to oscillate, almost reaching the left edge of the LDOS (i.e., the lattice site is nearly completely depleted) at time $t = 4$. The occupation energy at site $i_p = 3$ inside the nanoprobe is not defined at time $t = 0$ because the system is empty. However, after the probe is coupled to the sample, $E_{\text{occ}}(t)$ begins to oscillate, similarly to the value on site $i_s = 26$, which is directly coupled to this lattice site of the nanoprobe. The oscillations of $E_{\text{occ}}(t)$ on these two sites have approximately opposite phase, indicating strong tunneling of particles between the two lattice sites. This is to be expected, since at $U = 0$ there is no scattering between the particles, which could lead to equilibration of local observables on short time scales.

2. Interacting case at quarter filling

We now turn on the Hubbard interaction to $U = 4$, staying with quarter filling and resting nanoprobe, $v = 0$; see Fig. 3. As can be seen by comparing Fig. 3(a) with Fig. 2(a), the oscillation in local particle density between the system and the nanoprobe is more damped than in the $U = 0$ case. Again, a light cone that spreads out over the system with the speed $c \approx 1.6$ is clearly evident. Examining the LDOS for site $i_s = 13$ (well to the left of the nanoprobe), we obtain a double peak structure,

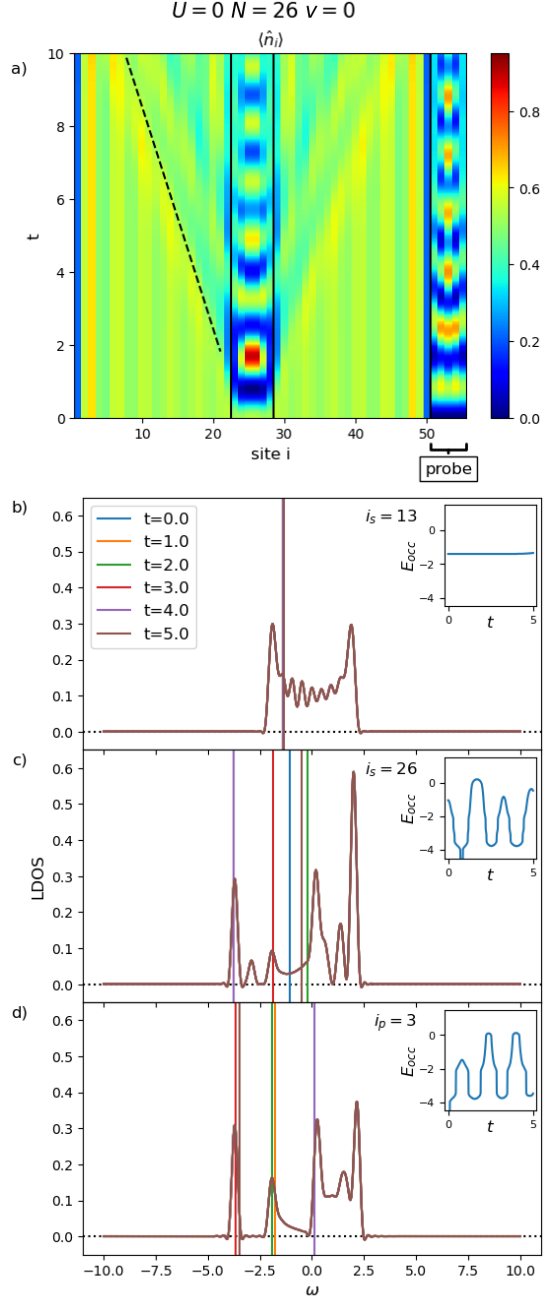


FIG. 2. Exact results for the nanoprobe model with $L = 50$ sample sites and $l = 5$ nanoprobe sites for the system initially at quarter filling, i.e., $N = 26$, with $U = 0$ and nanoprobe velocity $v = 0$. Here (a) depicts the expectation value of the local particle density, $\langle n_i \rangle$, as a function of lattice site i and time t , and (b), (c), and (d) plot the LDOS for the lattice sites $i_s = 13$, $i_s = 26$, and $i_p = 3$, respectively, as a function of the frequency ω . Note that the LDOS is rigorously time-independent for $U = 0$ when $v = 0$. The occupation energy $E_{\text{occ}}(t)$ is shown as an inset for each of the three lattice sites as a function of t and is also shown at five indicated times as vertical lines in the LDOS.

and an additional separated satellite peak at higher ω . Again, as in Fig. 2(b), $E_{\text{occ}}(t)$ is essentially time-independent on this lattice site on the time scales shown. As before, this is to be expected from the light-cone signal in $n_i(t)$, which reaches this position only after the times shown.

For lattice sites $i_s = 26$, Fig. 2(c), and $i_p = 3$, Fig. 2(d), the overall structure of the LDOS is similar at all times. However, in contrast to the noninteracting case, the LDOS is time-dependent at both sites. This is due to the interactions between the electrons. Interestingly, at the later times treated by us, they seem to settle to a stationary value, and the change in time is smaller than at the beginning of the evolution. Again, $E_{\text{occ}}(t)$ changes significantly in time on both sites and oscillates with the period of the oscillations of the local densities on these sites. The phase of the oscillation again shows a tendency to be opposite on both sites, but the electron-electron interaction now induces a damping.

Note that, as discussed in Sec. II, the resolution in ω is significantly lower than for the $U = 0$ case, so that finer structures are not resolvable. In addition, on general grounds, the interaction U leads to self-energy contributions, which tend to broaden out peaks in spectral functions relative to the noninteracting case.

3. Interacting case at half filling

We now consider the effect of changing the initial filling of the system to half filling. Figure 4 depicts the time evolution of the local particle density for the noninteracting ($U = 0$) half-filled system. In contrast to the quarter-filled case, Fig. 2(a), we can see that the oscillatory behavior is now spread across the whole nanoprobe rather than being concentrated in its center. As discussed in Sec. II C 3, the LDOS for the $U = 0$ case is independent of band filling. However, E_{occ} changes in time, as shown in Fig. 2.

At finite interaction, $U = 4$, Fig. 6(a) shows that the oscillations in the local particle den-

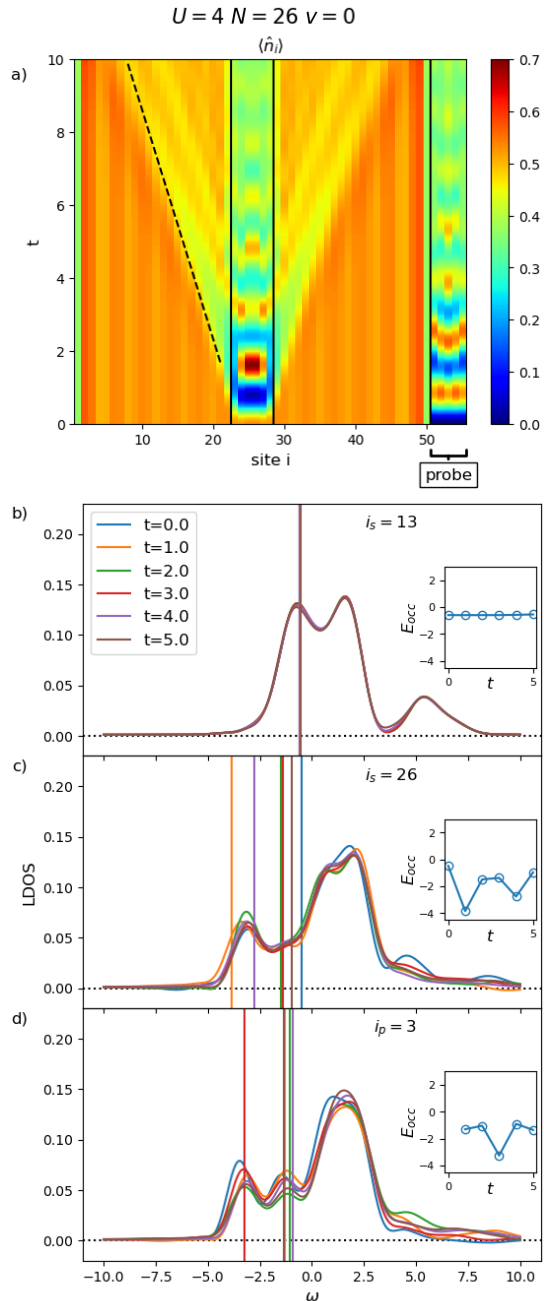


FIG. 3. MPS results for (a) the local particle density and the LDOS for (b) $i_s = 13$, (c) $i_s = 26$, and (d) $i_p = 3$, plotted as in Fig. 2, for $U = 4$, quarter filling, i.e., $N = 26$, and $v = 0$.

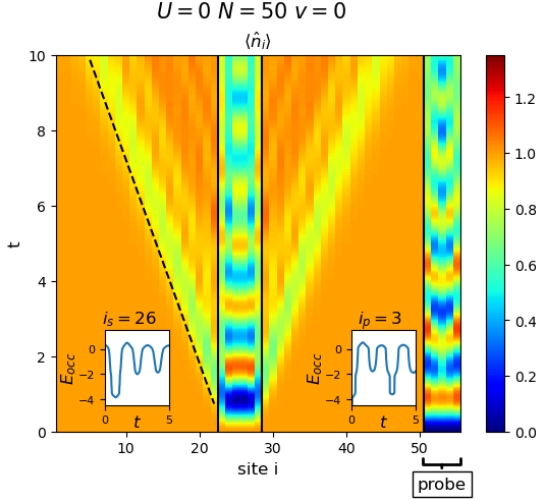


FIG. 4. Exact results for the local particle density plotted as in Fig. 2 for $U = 0$, half filling, i.e., $N = 50$, and $v = 0$. The occupation energy $E_{\text{occ}}(t)$ is shown as an inset for sites $i_s = 26$ and $i_p = 3$. The LDOS in this case is not explicitly shown, as it is the same as in Fig. 2.

sity between the sample and the nanoprobe are also present, but are heavily damped. The large damping is not unexpected, as the system is insulating for $U = 4$ and half filling, inhibiting charge transport.

In the LDOS at $i_s = 13$, Fig. 6(b), we observe two peaks, which, at the beginning of the time evolution, have essentially the same height. The splitting between the peaks is consistent with the size of the Mott-Hubbard gap at this value of U , which, according to the Bethe Ansatz, is $\Delta \approx 1.29$ [43]. However, note that the weight of the LDOS in Fig. 6 does not go to zero in the gap region. This is because of the limited resolution of our calculations; see Sec. II. As in the previously discussed cases, the LDOS and E_{occ} on this site initially show only very weak time dependence, while at $t = 5$ a clear change is visible. We associate this onset of change with the arrival of the light cone, which induces a change of the number of particles on this site, and hence a change of the LDOS and E_{occ} .

For $i_s = 26$ and $i_p = 3$, Figs. 6(c) and (d),

we obtain a continuous LDOS with a smaller peak at energies below E_{occ} and a higher peak at energies larger than E_{occ} . On both sites, the LDOS changes in time, while, at later times, the changes become smaller. The overall structure of the LDOS for both sites and at all times is again comparable, as in the case of quarter filling. However, the gap is no longer present after the coupling to the probe is turned on, indicating a melting of the Mott insulator in this region.

We expect that this melting of the Mott insulator will propagate through the system and that the gap in the LDOS will close with the arrival of the light cone on the respective site. It remains an open question as to whether the shape of the LDOS at longer times will approach the results on site $i_s = 26$ also further away from the nanoprobe. Due to the high computational cost, we do not address this question further in this paper.

From the insets of Figs. 6(b)-(d), it can be seen that $E_{\text{occ}}(t)$ behaves similarly to the previously discussed cases, but that the damping is much stronger. The behavior on sites $i_s = 26$ and $i_p = 3$ indicates that the amplitudes of the oscillations are damped nearly completely to zero on the time scales that we have been able to treat; in addition, the values of $E_{\text{occ}}(t)$ at time $t = 5$ are quite similar, which corresponds to what we would expect if equilibration takes place. Both aspects indicate that the LDOS reaches equilibrium on both adjacent sites on the short time scales treated here. This is interesting because, in typical materials, the hopping strength is $t_h \sim 1\text{eV}$, which translates to time scales $\mathcal{O}(1\text{fs})$, corresponding to one time unit in Fig. 6. Thus, equilibration after coupling a Mott insulator to a nanoprobe seems to happen on ultrafast time scales of a few fs. To further investigate the equilibration behavior of the Mott-insulating case, longer times and additional Mott-insulating systems would need to be treated, which, due to the high computational expense, is left as a subject for future research.

4. Interpretation of the results as a nonequilibrium LDOS

In the preceding discussion, we have tacitly interpreted our results as if we were dealing with an equilibrium or near-equilibrium setup (i.e., have applied linear response), so that the corresponding Fourier transform of the Green's function, Eq. (3), can be rewritten in terms of a Lehmann representation with explicitly positive weights. Out of equilibrium, the weights cannot be proven to be positive in general [49], so that, in principle, negative weights can appear. This makes it difficult to interpret the corresponding results as a time-dependent LDOS. However, as can be seen in Figs. 2-6, all of the weights calculated here are positive, up to small artifacts, which may be due, at least in part, to the way we compute the Fourier transform. Hence, for the cases treated so far, it appears reasonable to interpret the results as time-evolving LDOS.

This issue can be further investigated by studying the lesser and greater parts of the LDOS as defined in Eqs. (4) and (5), respectively. In equilibrium, the expectation is that $\int d\omega B_\sigma^<(\omega, x) = \langle n_{x,\sigma} \rangle$. Figure 5 shows results for the discrepancy between the two quantities in the out-of-equilibrium case for both the non-interacting and the interacting, $U = 4$, cases at half filling with a resting nanoprobe. The agreement between $\int d\omega B_\sigma^<(\omega, x)$ and the independently computed expectation values $\langle n_{x,\sigma}(t) \rangle$ at later times is within a few percent, thus substantiating our interpretation of $D_\sigma(\omega, x, t)$, as defined in Eq. (3), as a good approximation to the time evolution of the LDOS for the later times. Interestingly, for the interacting system, the discrepancy is smaller than for the noninteracting system. At shorter times, $t \approx 1$, however, the discrepancy can become as large as $\sim 30\%$. This shows that here the system is in a strongly out-of-equilibrium regime in which the interpretation of our results as a time-dependent LDOS must be treated with caution. Note that, in all cases, the absolute value of the discrepancy is very small; at times $t \approx 1$, however, the small particle numbers lead to a large relative discrepancy. The discrepancy in the actual values is

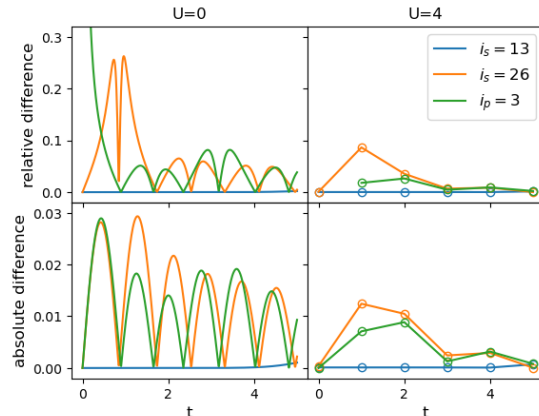


FIG. 5. Absolute and relative discrepancy between the local expectation value of the local densities $\langle n_{\sigma,x} \rangle(t)$ and the integral over the lesser spectral function $\int d\omega B_\sigma^<(\omega, x)$. Left column: half filling, i.e., $N = 50$, $U = 0$, $v = 0$. Right column: the same at $U = 4$. (Top row: relative difference, bottom row: absolute difference.) We define the absolute difference here as $|\int d\omega B_\sigma^<(\omega, x) - \langle n_{\sigma,x} \rangle(t)|$ and the relative difference as $|\int d\omega B_\sigma^<(\omega, x) / \langle n_{\sigma,x} \rangle(t) - 1|$.

larger at small times, and, again, is smaller for the interacting system.

For the case of a moving probe, similar behavior is obtained (see section III B and App. B). However, as we will see next, the computed LDOS can, in addition, take on negative values, in particular, in the strongly out-of-equilibrium regime at short times.

B. Moving nanoprobe: $v > 0$

Having explored the behavior when coupling a stationary nanoprobe to the sample at time $t = 0$, we now treat cases in which the nanoprobe is moving at constant speed. As in the stationary case, we also turn on the coupling between sample and a nanoprobe at the center of the sample at time $t = 0$; subsequently, the nanoprobe moves to the right relative to the sample with speed v .

A natural scale for the velocities in the sys-

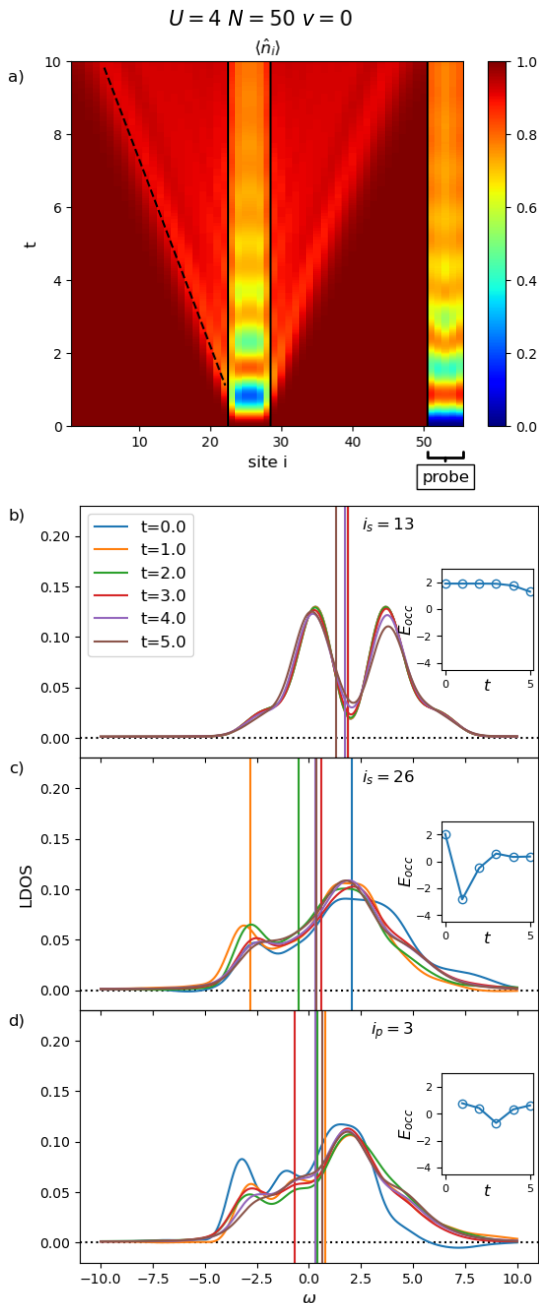


FIG. 6. MPS results for (a) the local particle density and the LDOS for (b) $i_s = 13$, (c) $i_s = 26$, and (d) $i_p = 3$, plotted as in Fig. 2, for $U = 4$, half filling, i.e., $N = 50$, and $v = 0$.

tem is the velocity of propagation of disturbances in the local particle density, i.e., the speed associated with the previously discussed light cone, $c \sim 2$. We treat two different velocities, $v = 0.55$ ($\approx c/4$) and $v = 1$ ($\approx c/2$). Here we present the findings for $v = 0.55$ in detail and complement the discussion by highlighting the similarities and differences with the case of the higher velocity of $v = 1$, for which we present additional results in App. B.

In the following, we will use the resting case, $v = 0$, as a reference, highlighting the similarities and differences of the behavior in the two moving cases. For all velocities $v > 0$, we find that there are stronger wave fronts to the left of the right-moving nanoprobe and weaker ones to its right, see, e.g., Fig. 7(a) for $v = 0.55$, $U = 0$, and quarter filling. Note that the slope of the wave fronts is still consistent with a constant speed $c \approx 1.6$ for the light cone. The effect of the movement of the probe is that particles “leak out” of the nanoprobe in the wake of its motion. The speed of $v = 0.55$ is an interesting case because, for this speed, we find that these “wake” effects are particularly pronounced, in contrast to the $v = 1$ case (see App. B). For $v = 0.55$, the motion of the probe is spatiotemporally commensurate with the oscillations of the particle density, which leads to constructive interference to the left of the moving probe. Therefore, the wave fronts are very pronounced for this particular velocity, as can be seen in Fig. 7(a). Strong oscillations in the local particle density between the nanoprobe and the system are still present, but, for the moving nanoprobe, they are mostly concentrated at its trailing edge rather than its center as in the stationary case.

The LDOS for this case is displayed in Figs. 7(b)–(d), for the same three sites as before, $i_s = 13$, $i_s = 26$, and $i_p = 3$. Note that the LDOS is now, in general, time-dependent, also for $U = 0$. As at $v = 0$, the LDOS at site $i_s = 13$ is essentially time-independent due to the fact that the nanoprobe is moving away from this site so that, at the times treated, the wake caused by the moving nanoprobe has not yet reached it. At site $i_s = 26$, Fig. 7(c),

the evolution of the LDOS differs significantly from that of the resting case, Fig. 2(c). One marked feature is that the results can now take on substantially negative values, in particular, for times $t < 3$. However, at later times, the discrepancy between $\langle n_{i,\sigma} \rangle$ and $\int d\omega B_\sigma^<(\omega)$ is only a few percent, a behavior similar to that of the case of the stationary nanoprobe. Note that $i_s = 26$ is a stationary point in the center of the sample and therefore becomes decoupled from the nanoprobe at time ≈ 6.4 , which is shorter than the time interval over which we perform the Fourier transform (from t to ω). For the faster moving case, $v = 1$, (see App. B), site $i_s = 26$ already decouples from the nanoprobe at times $t \approx 3.5$, so that the LDOS, Fig. 14(b), takes on, approximately, the decoupled equilibrium form, i.e., that of Fig. 2(b), for $t \geq 4$.

The LDOS at $i_p = 3$, Fig. 7(d), is essentially time-independent, despite the fast motion of the nanoprobe, a behavior also found in the $v = 1$ case; see App. B. The structure and the positions of the peaks are roughly the same as for the resting nanoprobe, Fig. 3(d). Regarding $E_{\text{occ}}(t)$, we see a similar behavior to that of the resting case for $i_s = 13$ and $i_p = 3$. However, $E_{\text{occ}}(t)$ appears to increase with time for $i_s = 26$, unlike in the resting case.

Turning on the interaction to $U = 4$ in the quarter-filled case with $v = 0.55$, Fig. 8, we see that $\langle n_i(t) \rangle$ has similar features to that of the $U = 0$ case, Fig. 7(a). Note, however, that now the oscillation is significantly more damped. As before, the LDOS at site $i_s = 13$, Fig. 8(b), is approximately time-independent since the light cone has not reached this position on the time scales treated by us. Comparing the LDOS on site $i_s = 26$ to the resting case, $v = 0$, we observe that the overall picture is comparable, but that there are now more changes in time in the relevant energy region; notably, at $t = 3$, a dip evolves between two peaks at $\omega \approx -2.5$ and $\omega \approx 1$. However, this dip disappears at later times. It is notable that—in contrast to the noninteracting case—the LDOS takes on (up to minimal effects) only positive values for all values of ω shown. As discussed in Section III A 4, the discrepancy of the occupations is only a few

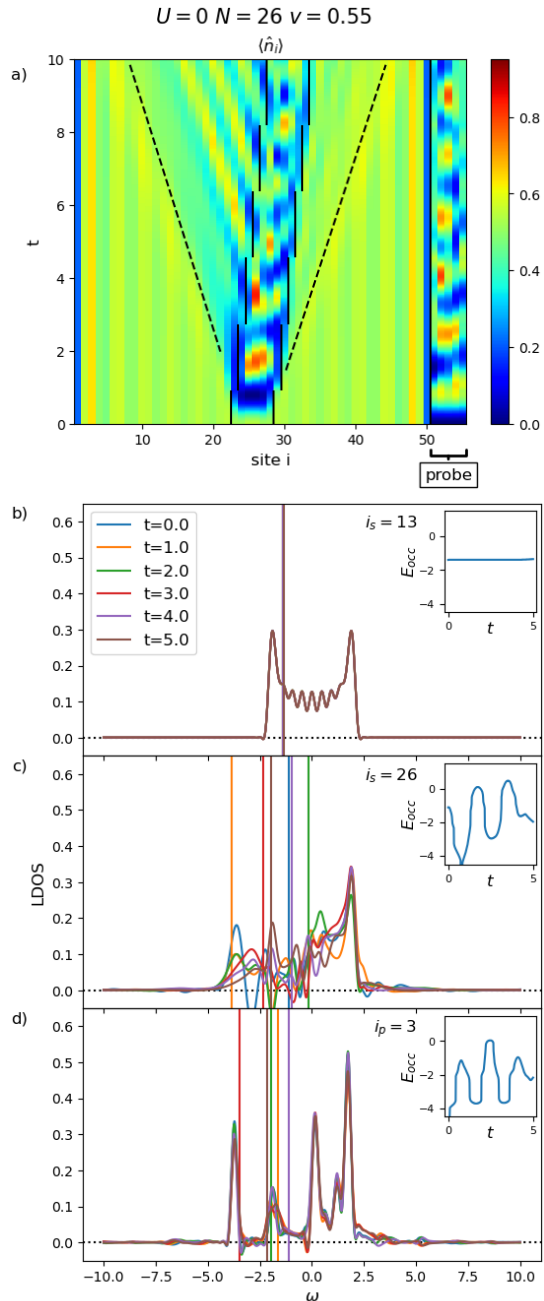


FIG. 7. Exact results for (a) the local particle density and the LDOS for (b) $i_s = 13$, (c) $i_s = 26$, and (d) $i_p = 3$, plotted as in Fig. 2, for $U = 0$, quarter filling, i.e., $N = 26$, and $v = 0.55$.

percent, so that, again, interpreting the spectrum as a quasi-equilibrium LDOS seems to be justified. For $i_p = 3$, Fig. 8(d), there is only weak time dependence. The results are very similar to the ones for $v = 0$, with only minor qualitative differences. This is interesting, as it indicates that the motion of the nanoprobe seems to not significantly affect the time evolution of the LDOS on its sites. This similarity of the LDOS on site $i_p = 3$ to the $v = 0$ case remains present when the nanoprobe velocity is higher, $v = 1$; see App. B.

The time-dependent behavior of $E_{\text{occ}}(t)$ for $v = 0.55$, depicted in the insets of Figs. 8(b)-(d), is very similar to that of the resting case, Figs. 3(b)-(d). However, for $i_s = 26$, $E_{\text{occ}}(t)$ appears to settle to a stationary value within the simulation time, in contrast to the $v = 0$ case. This difference in behavior is due to the fact that the probe moves away from this position so that local observables equilibrate faster than when the probe is resting. At site $i_p = 3$, however, $E_{\text{occ}}(t)$ keeps changing in time, as might be expected because the nanoprobe continues to move over the sample.

We continue examining probe velocity $v = 0.55$, but now increase the initial band filling to half filling, first taking $U = 0$. Figure 9 displays the $U = 0$ local particle density. As can be seen by comparing with Fig. 7(a), the wave fronts to the left of the nanoprobe are even more pronounced than in the quarter-filled case. Furthermore, there is an even stronger build-up of local particle density inside the probe. At larger times, the local particle density rapidly changes over to being concentrated at the leading edge of the nanoprobe. Note that the build-up of local density is even stronger in the $v = 1$ case, with it being concentrated at the trailing edge of the probe for times up to $t \approx 7$; see App. B.

We now consider the interacting case, $U = 4$, Fig. 10, remaining at half filling and $v = 0.55$. As in the half-filled, interacting, $v = 0$ case, Fig. 6(a), we see once again that the oscillation between the nanoprobe and the system is heavily damped. We notice that there is a lower particle density towards the left of the probe inside the light cone, consistent with the probe moving

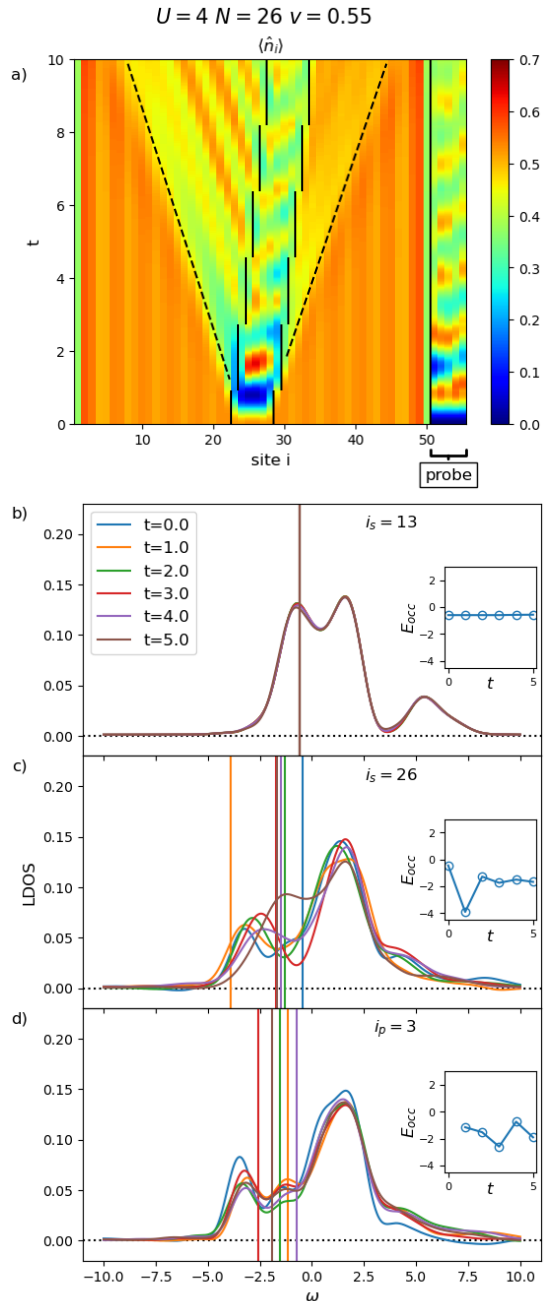


FIG. 8. MPS results for (a) the local particle density and the LDOS for (b) $i_s = 13$, (c) $i_s = 26$, and (d) $i_p = 3$, plotted as in Fig. 2, for $U = 4$, quarter filling, i.e., $N = 26$, and $v = 0.55$.

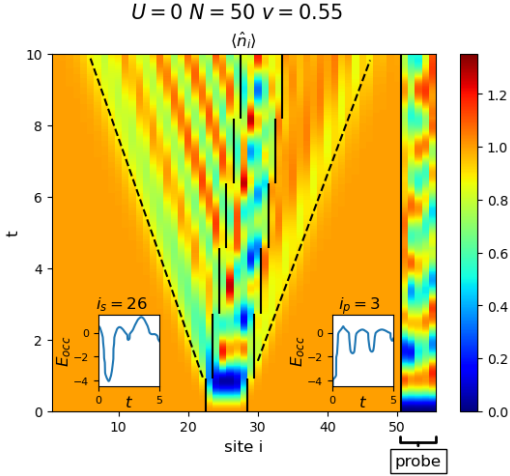


FIG. 9. Exact results for the local particle density, plotted as in Fig. 2, for $U = 0$, half filling, i.e., $N = 50$, and $v = 0.55$. The occupation energy $E_{\text{occ}}(t)$ is shown as an inset for sites $i_s = 26$ and $i_p = 3$. The LDOS in this case is not explicitly shown, as it is the same as in Fig. 7.

to the right. For higher probe velocity, $v = 1$ (see App. B), the local particle density behaves similarly, except that the oscillations in particle density in the sample are less strong, as the probe moves more quickly over the sample.

Examining the LDOS, first at site $i_s = 13$, Fig. 10(b), we can again see the peaks at $\omega \approx 0$ and $\omega \approx 4$ for $i_s = 13$ and a gap at $\omega \approx 2$, similar to the $v = 0$ case, Fig. 6(b). The movement of the probe causes the peak at $\omega \approx 4$ to shrink slightly for later times t , a feature also found at higher probe velocity $v = 1$ (see App. B). In the LDOS at site $i_s = 26$, Fig. 10(c), one can see that the Mott gap in the LDOS again disappears due to coupling to the empty nanoprobe. The LDOS features peaks at $\omega \approx -2.5$ and $\omega \approx 2$, and only changes slightly with time. At the latest time that we have reached, $t = 5$, the LDOS does show small changes, building up spectral weight between the two peaks. This is most likely due to the nanoprobe becoming decoupled from site $i_s = 26$ at $t \approx 6.4$, which is within the time interval over which the Fourier transform is carried out. This effect is not yet

noticeable at $t = 4$, probably because the Hann window that we apply weights times closer to the lower bound of the integral more strongly. At the initial time, $t = 0$, the LDOS at probe site $i_p = 3$, Fig. 10(d), exhibits peaks at $\omega \approx -4$ and $\omega \approx 2$. For $t \geq 1$, both peaks diminish slightly, and the LDOS is shifted a small amount towards larger ω values. The LDOS then appears to settle in to this slightly altered shape for all times $t \geq 1$. Interestingly, this form closely resembles that of the $i_s = 26$ LDOS, cf. Fig. 10(c), which seems reasonable because the two sites are directly connected via a hopping term.

Examining the behavior of $E_{\text{occ}}(t)$ [insets of Figs. 10(b), (c), and (d)], it appears to be heavily damped in time, similarly as in the stationary ($v = 0$) half-filled system, Figs. 6(b), (c), and (d). For $i_s = 26$ and $i_p = 3$, $E_{\text{occ}}(t)$ seems to settle to approximately the same value, which is slightly larger than zero.

IV. DISCUSSION AND SUMMARY

In this work, we have investigated the coupling of an empty nanoprobe to a one-dimensional system of correlated electrons for two different fillings, half filling and quarter filling, treating the case of a stationary nanoprobe as well as that of a moving one. We have taken both the sample and the nanoprobe to have intermediate local Coulomb interaction strength, $U = 4$, and have contrasted the behavior with that of the noninteracting, $U = 0$, case. In all scenarios that we have studied, the coupling between the sample and the nanoprobe, consisting of nearest-neighbor hopping terms between proximate lattice sites of the sample and corresponding sites of the nanoprobe, is suddenly turned on. Using an MPS formulation of the DMRG and treating the time dependence using an TDVP scheme, we have studied the time-dependent behavior of the local particle density $\langle n_i \rangle(t)$ and of the LDOS $D_\sigma(t, \omega, x)$, as defined by Eq. (3).

As a reference system, we take the noninteracting case with a stationary nanoprobe. Turn-

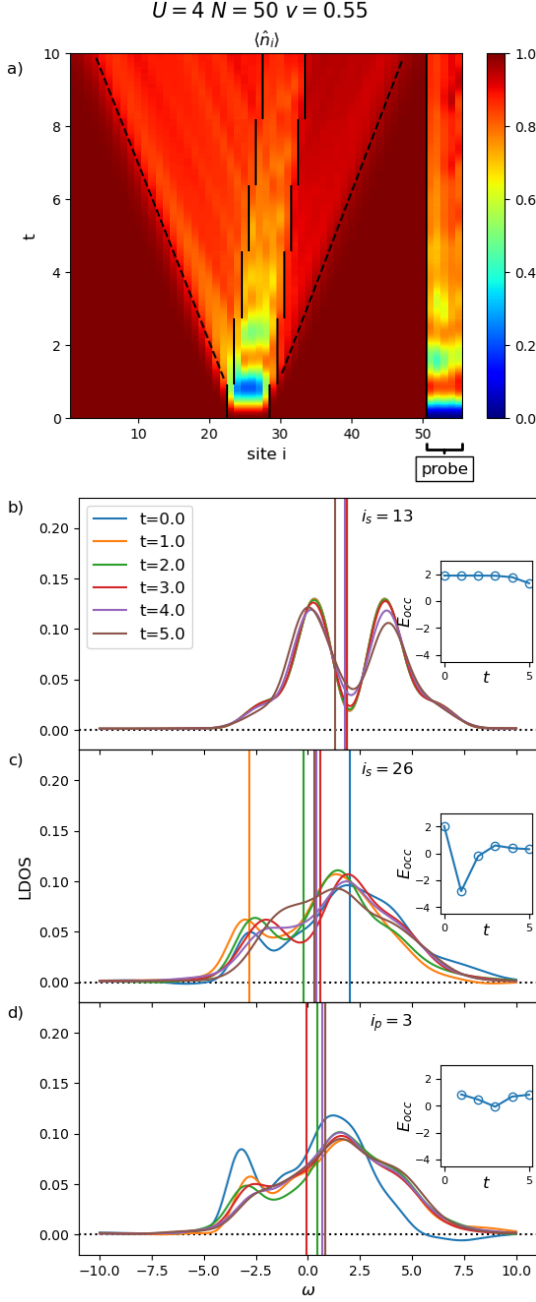


FIG. 10. MPS results for (a) the local particle density and the LDOS for (b) $i_s = 13$, (c) $i_s = 26$, and (d) $i_p = 3$, plotted as in Fig. 2, for $U = 4$, half filling, i.e., $N = 50$, and $v = 0.55$.

ing on the hopping between the sample and the empty nanoprobe at $t = 0$ induces long-lived oscillations in the local particle density $\langle n_i \rangle(t)$ in the sites in the probe and in the sample in the vicinity of the nanoprobe. As can be shown rigorously, the LDOS for this system is time-independent. However, the occupation energy $E_{occ}(t)$, defined by Eq. (8), which is a measure of the local chemical potential, oscillates in time, with opposing phases of oscillation on the site on the nanoprobe and the proximate site on the sample due to the strong tunneling between them, reflecting the oscillations in the local particle density.

For systems with finite interaction strength, $U = 4$, oscillations in the local particle density are still present, but become more strongly damped, especially at half filling. At both quarter and half filling, the LDOS is no longer time-independent, but does evolve towards a stationary form at longer times; this holds for both stationary and moving nanoprobes. The oscillations in $E_{occ}(t)$ are, in general, still present, but are more strongly damped than for $U = 0$, indicating that the system seems to already attain local equilibrium on the short time scales that we have been able to treat here. This damping is somewhat stronger for the half-filled case than for the quarter-filled one, reflecting the reduced charge mobility in the initially Mott insulating phase, consistent with the stronger damping in the local particle density.

For the initially half-filled sample, the gap in the LDOS in the sample site situated at the center of the nanoprobe closes immediately upon suddenly coupling the sample and probe, indicating the local breakdown of the Mott insulator. However, for sample sites further away from the nanoprobe, some time is required before the perturbation induced by coupling the two subsystems reaches the observation position. In this way, one observes a “melting” of the Mott insulator that propagates through the system with time. For the quarter-filled sample, the LDOS is clearly metallic far from the nanoprobe, where it remains stationary, in the sample under the nanoprobe, where there is moderate change with time, and in the

nanoprobe, where there are only small changes with time once the connection between sample and probe is turned on.

For a moving nanoprobe, the local environment in the sample, in particular, the local particle density, changes as the nanoprobe moves over it. Note, however, that changes in the sample propagate outwards with a velocity given by the light cone, which is significantly larger than the speed of movement of the nanoprobe and can be clearly seen in the time and space dependence of the local particle density. The primary effect of the movement of the nanoprobe is to reduce backflow effects into the sample, as the back-tunneling from the probe to the sample is spread over different sample sites as the probe moves. The behavior of the LDOS is similar to that of the case of a resting nanoprobe. Interestingly, on the sites of the moving probe, the LDOS behaves essentially as if the probe were at rest. On the sites in the sample, the behavior of the LDOS is similar to that in the stationary case, up to times at which the site initially under the nanoprobe is no longer under the influence of the nanoprobe because it moves far enough away.

These features of the cases with a moving nanoprobe remain qualitatively the same when the speed of the nanoprobe is increased. The exceptions are that for the slower nanoprobe velocity, $v = 0.55$, there are interference effects in the local particle density due to commensuration of spatial and temporal oscillations of the local particle density that are not present at the higher nanoprobe speed, $v = 1$. In addition, the decoupling of the nanoprobe from sample sites initially under the nanoprobe occurs on shorter time scales for the fast nanoprobe velocity, so that quasi-equilibration of the LDOS occurs sooner on such sites.

We remark that the nonequilibrium LDOS that we have computed [Eq. (3)] is not restricted to be strictly positive semi-definite. Negative values are incompatible with the interpretation as spectral weights that one is used to for an equilibrium LDOS. However, we, in fact, find that negative weights only occur in very few cases (most markedly, in the $U = 0$

case with a moving nanoprobe), and, for these cases, only at short times. In these cases, we also find that there is a discrepancy between the local particle density directly calculated as $\langle n_{i,\sigma} \rangle(t)$ and that obtained from $\int d\omega B_\sigma^<(\omega)$. We characterize this anomalous short-time behavior as being strongly nonequilibrium. Thus, the general picture is that the discrepancies in the local particle density and the appearance of negative values of the LDOS disappear at later times (especially in the interacting system), which is consistent with reaching an equilibrium state, so that a description in terms of standard linear response theory is applicable. It is interesting to see that this happens on the very short time scales treated by us; for a typical material, the hopping strength $t_h \sim 0.5 - 1$ eV. Since the units of our time scale are \hbar/t_h , this implies that our calculations typically reach $\sim 5 - 10$ fs, which lies in the ultrafast regime of even highly time-resolved experimental techniques such as pump-probe experiments. Developing such time-resolved local spectroscopy with STM is an ongoing challenge [62]. However, one can envisage that similar scenarios to the ones proposed here could be studied using single-site microscopes in experiments on optical lattices, which realize the Hubbard model [63–67]. In either case, it will be interesting to study how the states developing on the ultrashort time scales treated by us here affect the behavior at the later times accessible to these experiments.

It would therefore be interesting to also study the time evolution of the LDOS and other dynamical quantities for other strongly correlated systems. For example, investigating a similar scenario to the one treated here in correlated charge density wave (CDW) insulators could allow one to study if and how the melting of a CDW state propagates through the system after a local perturbation. Since topological phases are either protected by local symmetries (e.g., symmetry-protected topological phases in 1D), or by long-range entanglement (in particular, in 2D systems), it would be interesting to study the interplay of the local perturbation with these protection mechanisms by studying

the time evolution of the LDOS.

ACKNOWLEDGMENTS

We thank Martin Wenderoth for helpful discussions. SRM acknowledges financial support by the Deutsche Forschungsgemeinschaft (DFG, German Research Foundation) - 217133147/SFB 1073, project B03 and by Philipps-Universität Marburg through a visiting professorship from 2020-21.

Appendix A: Numerical Accuracy

The truncation error of the time evolution has been found to be proportional to the square root of the discarded weight: $\epsilon \approx \sqrt{\delta}$ [58]. In Fig. 11, we find that, for the half-filled system, the discarded weight for later times reaches just under $\delta \approx 10^{-4}$, resulting in an error of $\approx 10^{-2}$. This level of accuracy should be sufficient to discern features of the LDOS that dominate its qualitative behavior. Furthermore, as discussed in Sec. II C, this level of error is also overshadowed by the limited resolution of our calculation of the LDOS caused by the fact that we are only able to carry out the integrals in Eqs. (4) and (5) to $\tau_{\max} = 5$.

In Fig. 12(a), it can be seen that the error in the local particle density $\langle n_i \rangle$ becomes appreciable at times after $t \approx 4$ in and in the vicinity of the nanoprobe and continues to grow and spread out as time progresses. The error is thus concentrated in regions in which the most change in time takes place. The LDOS far away from the nanoprobe, $i_s = 13$, Fig. 12(b), shows no significant error, whereas that under and in the nanoprobe, Figs. 12(c)-(d) shows absolute errors that grow with time, becoming significant at later times. Nevertheless, we consider them to be small enough to ensure that the qualitative behavior of the LDOS, which is limited anyway due to taking the maximum time in our Fourier integration, Eqs. (4) and (5), to be $\tau_{\max} = 5$. The maximum absolute difference in the LDOS at sites $i_s = 26$ and $i_p = 3$ for later

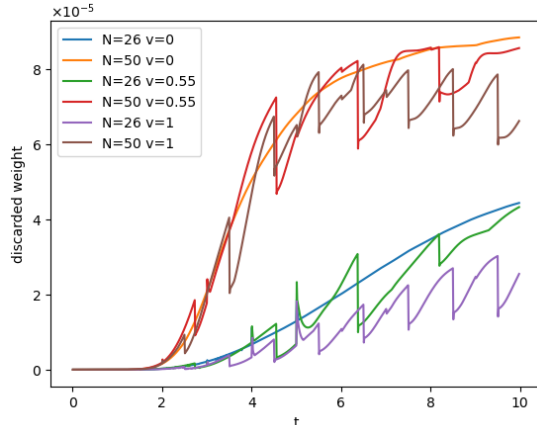


FIG. 11. Maximum discarded weight δ during a TDVP time step as a function of the evolution time t for $U = 4$, with $L = 50$ sample sites and $l = 5$ nanoprobe sites and initial filling and probe speed as indicated in the legend.

times is about 0.014. The largest peaks that are resolved in the LDOS (for $\tau_{\max} = 5$) are approximately 0.15 in amplitude. This is an error of about 10% for the largest peaks and only occurs at later times. Despite this appreciable error, the accuracy should be sufficient to resolve the larger peaks in the LDOS. When evaluating the presence and size of the smallest peaks, however, which reach from approximately 0.015 to 0.05, one cannot necessarily make a definite determination. Nevertheless, we emphasize that the errors at smaller times and for lattice site $i_s = 13$ are almost negligible and yield more than sufficiently accurate results.

Appendix B: Results for $v = 1$

In this appendix, we present results for a probe velocity of $v = 1$ for the same sets of remaining parameters as the results for $v = 0.55$ presented in Sec. III B. Note that most of the features of the $v = 1$ case are very similar to those of the $v = 0.55$ case; many of the important differences and similarities have already been highlighted in Sec. III B. In the following,

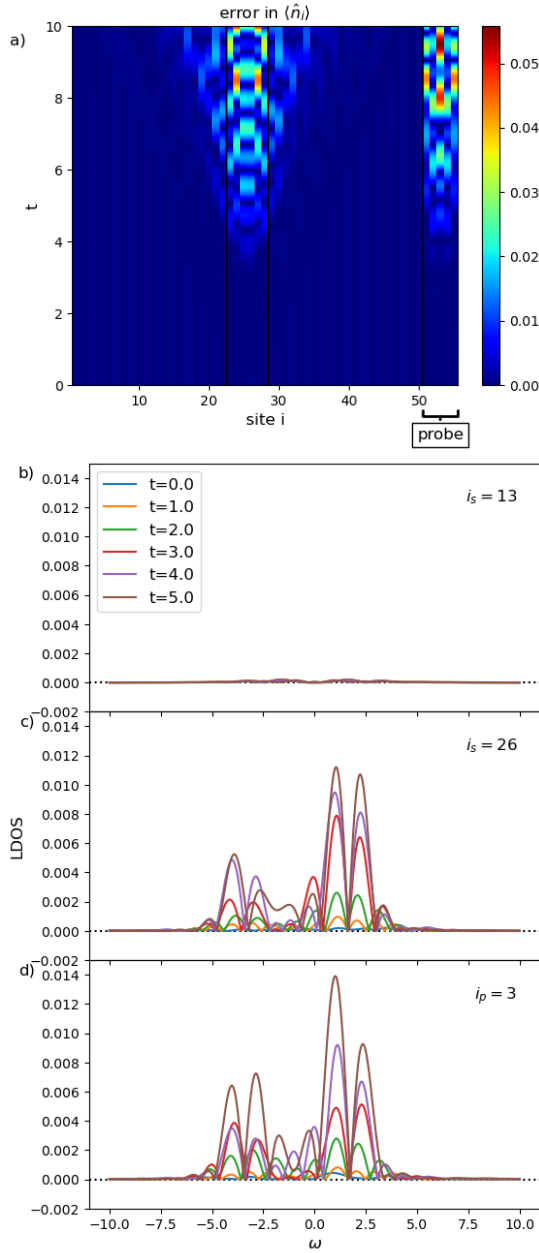


FIG. 12. Results of the TDVP time evolution, with $L = 50$ sample sites and $l = 5$ nanoprobe sites, compared to exact diagonalization for $U = 0$ and probe velocity $v = 0$ at half filling, i.e., $N = 50$. Here (a) depicts the absolute difference in the particle density $\langle n_i \rangle$, and (b)-(d) depict the absolute difference in the LDOS at the indicated sites. Note that the maximum integration time $\tau_{\max} = 5$ for both the exact diagonalization and TDVP calculations in order to make the results comparable.

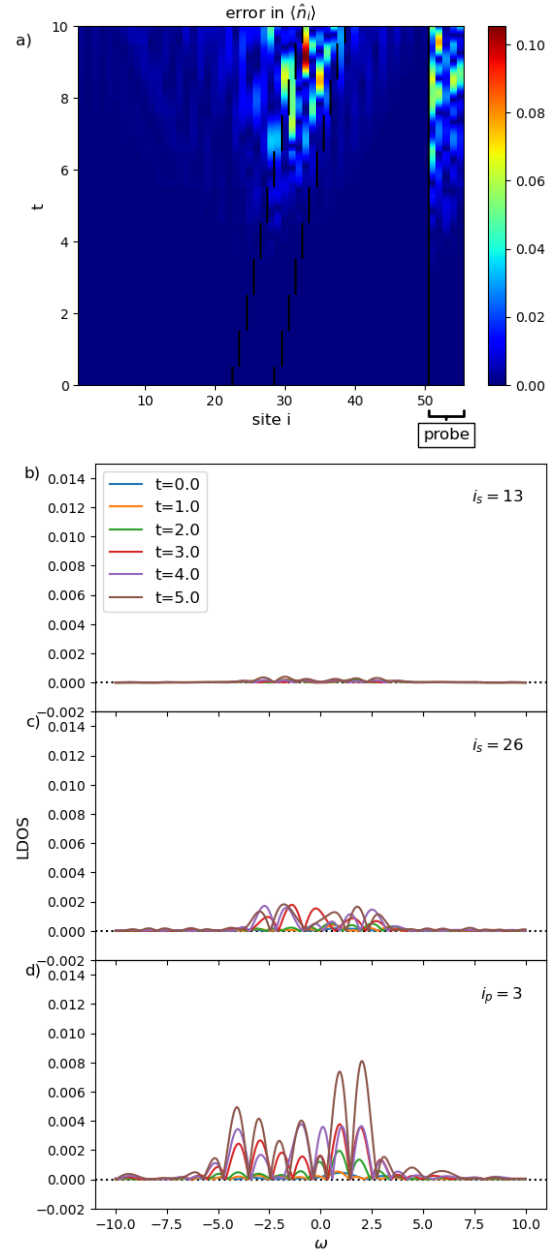


FIG. 13. Results of the TDVP time evolution compared to exact diagonalization as in Fig. 12, except for probe velocity $v = 1$.

we will present $v = 1$ results for both quarter and half filling for both $U = 0$ and $U = 4$ and briefly describe salient aspects.

We first treat the case of zero interaction strength, $U = 0$, and quarter filling. Comparing the local particle density, Fig. 14(a), with that for the $v = 0.55$ case, Fig. 7(a), we observe the same qualitative behavior, albeit with more pronounced wave fronts to the left of the nanoprobe for $v = 0.55$, as discussed in Sec. III B. Comparing the LDOS for sample site $i_s = 26$, Fig. 14(b), to that of the $v = 0.55$ case, Fig. 7(c), we can see that the right peak in the LDOS is preserved throughout the whole time evolution. However, the left peak in Fig. 7(b) is lost after the coupling of the probe to the system is turned on at $t = 0$. Note, however, that this peak is restored at $t \approx 3.5$ for $v = 1$, as can be seen in Fig. 14(b). This is due to the fact that, at this point in time, the probe has traveled far enough across the system that site $i_s = 26$ is decoupled from the probe.

We now turn to the case of intermediate interaction strength, $U = 4$, for the quarter-filled system. Comparing the local particle density, Fig. 15(a), with that for the $v = 0.55$ case, Fig. 8(a), we again see mostly the same behavior except that there are more pronounced wave fronts to the left of the nanoprobe. For the LDOS, comparing Figs. 15 (b)-(d), with Figs. 8 (b)-(d), we can see that the LDOS at sites $i_s = 13$ and $i_p = 3$ are almost unaffected by the change in speed of the probe. In Fig. 15 (c), we again observe that the left peak in the LDOS is restored for times $t \geq 4$ for the probe speed of $v = 1$ due to decoupling of the nanoprobe from site $i_s = 26$.

For the $U = 0$ case in the half-filled system, comparing Fig. 16 with Fig. 9, the behavior is qualitatively the same except for the more pronounced wave fronts for $v = 0.55$, also seen at quarter filling. One can see that there are more particles collected in the nanoprobe over time for $v = 1$; this is due to the fact that the higher probe speed makes more particles available to tunnel into the probe.

Finally, for interaction strength $U = 4$ and half filling, comparing Fig. 17 with the $v =$

0.55 case, Fig. 10, the local particle density, Fig. 17(a), behaves similarly for the two probe speeds, but again, more particles are collected in the probe over time for $v = 1$. In the LDOS, the behavior for site $i_s = 13$, Fig. 17(b), is essentially unaffected by the probe speed, showing a double-peak structure characteristic of a Mott insulator where there is only a slight shift in the relative weight of the two peaks with time. For site $i_s = 26$, the behavior at $v = 1$, Fig. 17(c), is similar to that for $v = 0.55$, Fig. 10(c), in that the two-peak structure characterizing the Mott insulator immediately disappears at $t = 0$, and two weaker peaks at small times evolve into a structure characterized by one peak. In contrast to $v = 0.55$, however, a new two-peak structure with a stronger, broader, left peak, emerges and remains stationary at the two longest times, $t = 4.0$ and $t = 5.0$. Within the nanoprobe at $i_p = 3$, the behavior for $v = 1$, Fig. 17(d), and $v = 0.55$, Fig. 10(c), is virtually identical, showing a two-peak structure without a discernible gap at small times washing out into a broad structure with vestigial peaks at larger times.

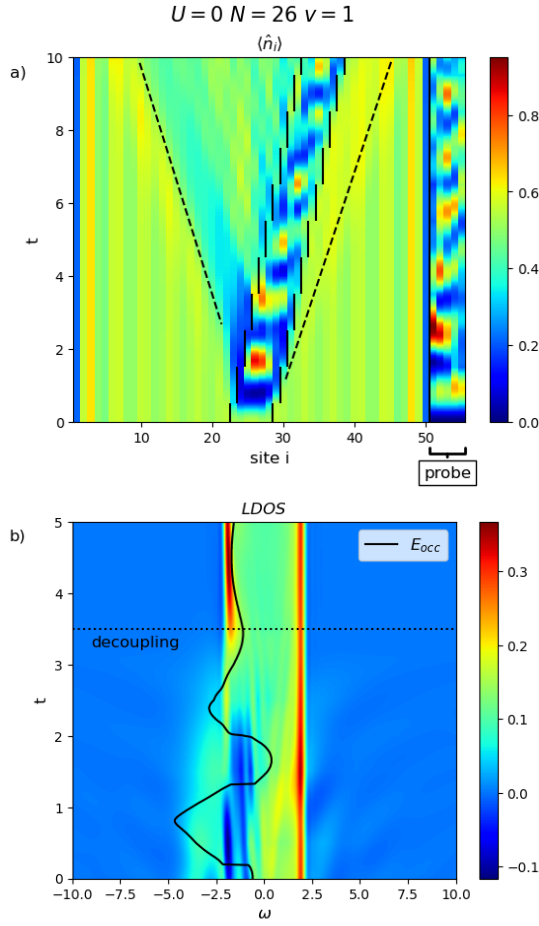


FIG. 14. Exact results for the nanoprobe model, with $L = 50$ sample sites and $l = 5$ nanoprobe sites, for the system initially at quarter filling, i.e., $N = 26$, with $U = 0$ and nanoprobe velocity $v = 1$. Here (a) depicts the expectation value of the local particle density, $\langle n_i \rangle$ as a function of lattice site i and time t , and (b) plots the LDOS at site $i_s = 26$ as a function of the frequency ω . The occupation energy $E_{\text{occ}}(t)$ at site $i_s = 26$ is shown as a solid line. The dotted line indicates the decoupling of the probe from lattice site $i_s = 26$ at $t = 3.5$.

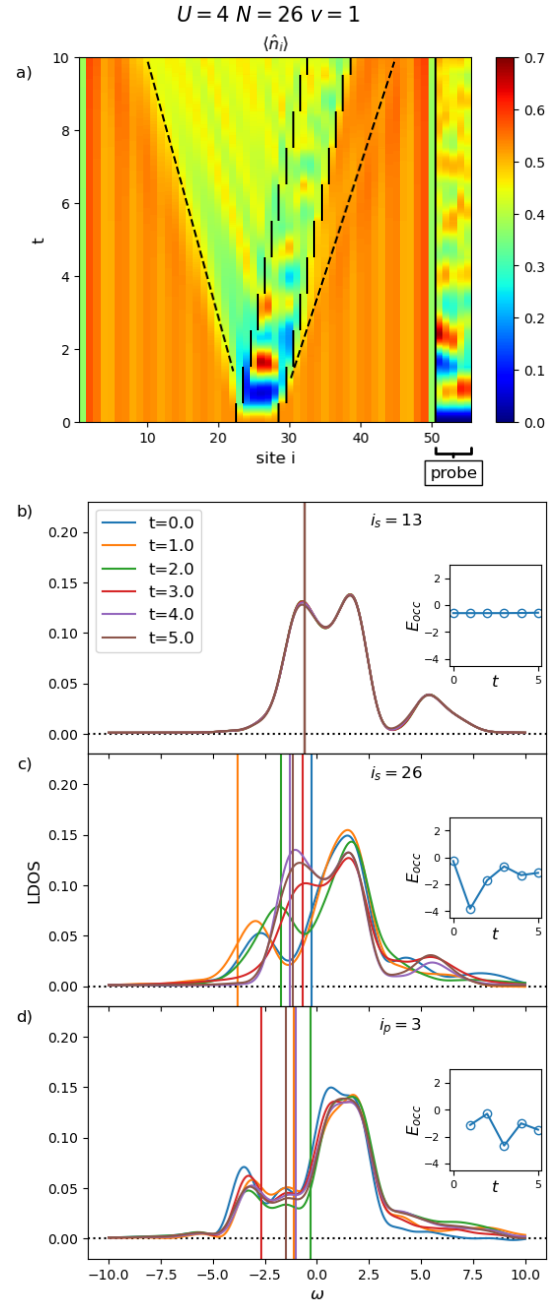


FIG. 15. MPS results for (a) the local particle density and the LDOS for (b) $i_s = 13$, (c) $i_s = 26$, and (d) $i_p = 3$, plotted as in Fig. 2, for $U = 4$, quarter filling, i.e., $N = 26$, and $v = 1$.

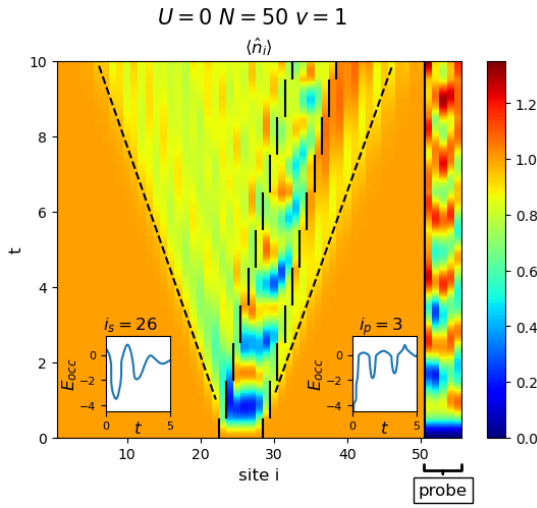


FIG. 16. Exact results for the local particle density, plotted as in Fig. 2, for $U = 0$, half filling, i.e., $N = 50$, and $v = 1$. The occupation energy $E_{\text{occ}}(t)$ is shown as an inset for sites $i_s = 26$ and $i_p = 3$. The LDOS in this case is not explicitly shown, as it is the same as in Fig. 14.

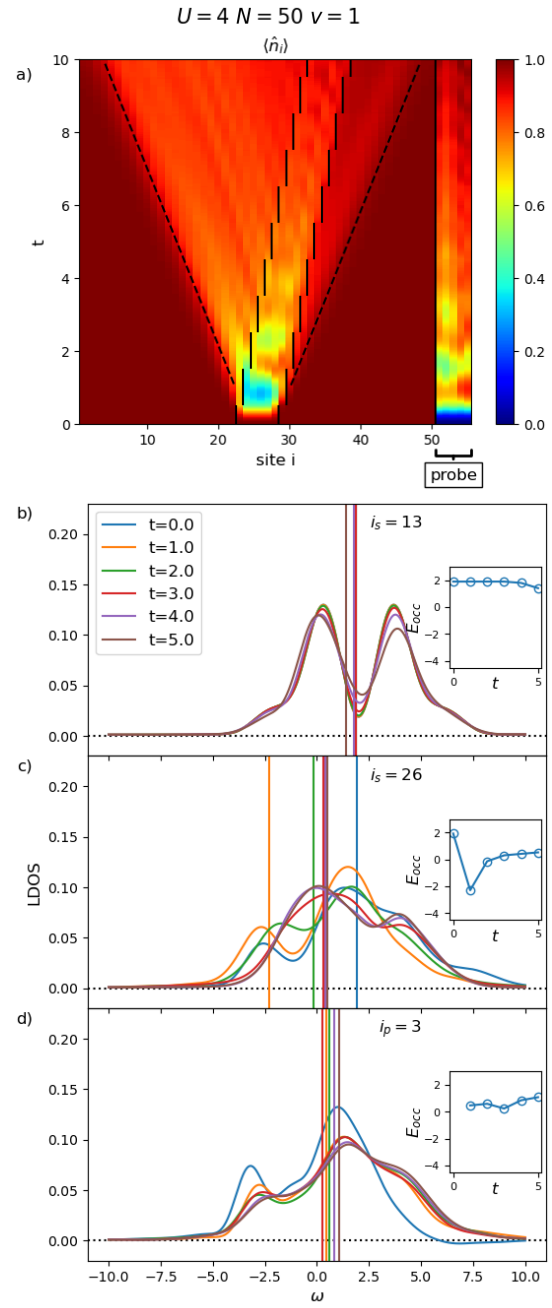


FIG. 17. MPS results for (a) the local particle density and the LDOS for (b) $i_s = 13$, (c) $i_s = 26$, and (d) $i_p = 3$, plotted as in Fig. 2, for $U = 4$, half filling, i.e., $N = 50$, and $v = 1$.

-
- [1] M. Rigol, V. Dunjko, and M. Olshanii, Thermalization and its mechanism for generic isolated quantum systems, *Nature* **452**, 854 (2008).
- [2] R. Nandkishore and D. A. Huse, Many-Body Localization and Thermalization in Quantum Statistical Mechanics, *Annual Review of Condensed Matter Physics* **6**, 15 (2015).
- [3] L. D'Alessio, Y. Kafri, A. Polkovnikov, and M. Rigol, From quantum chaos and eigenstate thermalization to statistical mechanics and thermodynamics, *Advances in Physics* **65**, 239 (2016).
- [4] T. Mori, T. N. Ikeda, E. Kaminishi, and M. Ueda, Thermalization and prethermalization in isolated quantum systems: a theoretical overview, *Journal of Physics B: Atomic, Molecular and Optical Physics* **51**, 112001 (2018).
- [5] I. Bloch, J. Dalibard, and W. Zwerger, Many-body physics with ultracold gases, *Rev. Mod. Phys.* **80**, 885 (2008).
- [6] C. Gross and I. Bloch, Quantum simulations with ultracold atoms in optical lattices, *Science* **357**, 995 (2017).
- [7] P. Baum, D.-S. Yang, and A. H. Zewail, 4D Visualization of Transitional Structures in Phase Transformations by Electron Diffraction, *Science* **318**, 788 (2007).
- [8] F. Krausz and M. Ivanov, Attosecond physics, *Rev. Mod. Phys.* **81**, 163 (2009).
- [9] J. K. Freericks, H. R. Krishnamurthy, and T. Pruschke, Theoretical Description of Time-Resolved Photoemission Spectroscopy: Application to Pump-Probe Experiments, *Phys. Rev. Lett.* **102**, 136401 (2009).
- [10] J. K. Freericks, H. R. Krishnamurthy, M. A. Sentef, and T. P. Devereaux, Gauge invariance in the theoretical description of time-resolved angle-resolved pump/probe photoemission spectroscopy, *Physica Scripta* **2015**, 014012 (2015).
- [11] A. Tomeljak, H. Schäfer, D. Städter, M. Beyer, K. Biljakovic, and J. Demsar, Dynamics of Photoinduced Charge-Density-Wave to Metal Phase Transition in $\text{K}_{0.3}\text{MoO}_3$, *Phys. Rev. Lett.* **102**, 066404 (2009).
- [12] S. Vogelgesang, G. Storeck, J. G. Horstmann, T. Diekmann, M. Siviš, S. Schramm, K. Rossnagel, S. Schäfer, and C. Ropers, Phase ordering of charge density waves traced by ultrafast low-energy electron diffraction, *Nature Physics* **14**, 184 (2018).
- [13] C. Laulhé *et al.*, Ultrafast Formation of a Charge Density Wave State in $1T\text{-TaS}_2$: Observation at Nanometer Scales Using Time-Resolved X-Ray Diffraction, *Phys. Rev. Lett.* **118**, 247401 (2017).
- [14] L. Stojchevska, I. Vaskivskyi, T. Mertelj, P. Kusar, D. Svetin, S. Brazovskii, and D. Mihailovic, Ultrafast Switching to a Stable Hidden Quantum State in an Electronic Crystal, *Science* **344**, 177 (2014).
- [15] S. Mathias *et al.*, Self-amplified photo-induced gap quenching in a correlated electron material, *Nature Communications* **7**, 12902 (2016).
- [16] S. Hellmann *et al.*, Time-domain classification of charge-density-wave insulators, *Nature Communications* **3**, 1069 (2012).
- [17] T. Rohwer *et al.*, Collapse of long-range charge order tracked by time-resolved photoemission at high momenta, *Nature* **471**, 490 (2011).
- [18] F. Schmitt *et al.*, Transient Electronic Structure and Melting of a Charge Density Wave in TbTe_3 , *Science* **321**, 1649 (2008).
- [19] A. Singer *et al.*, Photoinduced Enhancement of the Charge Density Wave Amplitude, *Phys. Rev. Lett.* **117**, 056401 (2016).
- [20] L. Rettig, R. Cortés, J. H. Chu, I. R. Fisher, F. Schmitt, R. G. Moore, Z. X. Shen, P. S. Kirchmann, M. Wolf, and U. Bovensiepen, Persistent order due to transiently enhanced nesting in an electronically excited charge density wave, *Nature Communications* **7**, 10459 (2016).
- [21] T. Eggebrecht, M. Möller, J. G. Gatzmann, N. Rubiano da Silva, A. Feist, U. Martens, H. Ulrichs, M. Münzenberg, C. Ropers, and S. Schäfer, Light-Induced Metastable Magnetic Texture Uncovered by in situ Lorentz Microscopy, *Phys. Rev. Lett.* **118**, 097203 (2017).
- [22] M. Rini, R. Tobey, N. Dean, J. Itatani, Y. Tomioka, Y. Tokura, R. W. Schoenlein, and A. Cavalleri, Control of the electronic phase of a manganite by mode-selective vibrational excitation, *Nature* **449**, 72 (2007).
- [23] E. Collet *et al.*, Laser-Induced Ferroelectric Structural Order in an Organic Charge-Transfer Crystal, *Science* **300**, 612 (2003).
- [24] D. Fausti, R. I. Tobey, N. Dean, S. Kaiser, A. Dienst, M. C. Hoffmann, S. Pyon,

- T. Takayama, H. Takagi, and A. Cavalleri, Light-Induced Superconductivity in a Stripe-Ordered Cuprate, *Science* **331**, 189 (2011).
- [25] F. Boschini, M. Zonno, and A. Damascelli, Time-resolved ARPES studies of quantum materials, *Rev. Mod. Phys.* **96**, 015003 (2024).
- [26] Y. H. Wang, H. Steinberg, P. Jarillo-Herrero, and N. Gedik, Observation of Floquet-Bloch States on the Surface of a Topological Insulator, *Science* **342**, 453 (2013).
- [27] F. Mahmood, C.-K. Chan, Z. Alpichshev, D. Gardner, Y. Lee, P. A. Lee, and N. Gedik, Selective Scattering between Floquet-Bloch and Volkov States in a Topological Insulator, *Nature Physics* **12**, 306 (2016).
- [28] T. Oka and S. Kitamura, Floquet Engineering of Quantum Materials, *Annual Review of Condensed Matter Physics* **10**, 387 (2019).
- [29] D. N. Basov, R. D. Averitt, and D. Hsieh, Towards properties on demand in quantum materials, *Nature Materials* **16**, 1077 (2017).
- [30] A. de la Torre, D. M. Kennes, M. Claassen, S. Gerber, J. W. McIver, and M. A. Sentef, Colloquium: Nonthermal pathways to ultrafast control in quantum materials, *Rev. Mod. Phys.* **93**, 041002 (2021).
- [31] M. Rodriguez-Vega, M. Vogl, and G. A. Fiete, Low-frequency and Moiré-Floquet engineering: A review, *Annals of Physics* **435**, 168434 (2021), special issue on Philip W. Anderson.
- [32] S. Ito *et al.*, Build-up and dephasing of Floquet-Bloch bands on subcycle timescales, *Nature* **616**, 696 (2023).
- [33] M. Merboldt *et al.*, Observation of Floquet states in graphene, arXiv:2404.12791.
- [34] D. Choi, M. Mogi, U. D. Giovannini, D. Azoury, B. Lv, Y. Su, H. Hübener, A. Rubio, and N. Gedik, Direct observation of Floquet-Bloch states in monolayer graphene, arXiv:2404.14392.
- [35] A. Eckardt, Colloquium: Atomic quantum gases in periodically driven optical lattices, *Rev. Mod. Phys.* **89**, 011004 (2017).
- [36] T. Oka and S. Kitamura, Floquet Engineering of Quantum Materials, *Annual Review of Condensed Matter Physics* **10**, 387 (2019).
- [37] D. Schmitt *et al.*, Formation of moiré interlayer excitons in space and time, *Nature* **608**, 499 (2022).
- [38] G. Binnig and H. Rohrer, Scanning tunneling microscopy—from birth to adolescence, *Rev. Mod. Phys.* **59**, 615 (1987).
- [39] Scanning Probe Microscopy: From Sublime to Ubiquitous, *Phys. Rev. Lett. Collection*, <https://journals.aps.org/prl/scanning-probe-microscopy>.
- [40] B. Bertini, F. Heidrich-Meisner, C. Karrasch, T. Prosen, R. Steinigeweg, and M. Žnidarič, Finite-temperature transport in one-dimensional quantum lattice models, *Rev. Mod. Phys.* **93**, 025003 (2021).
- [41] J. Hubbard, Electron Correlations In Narrow Energy Bands, *Proc. R. Soc. Lond. A* **276**, 238 (1963).
- [42] F. H. L. Essler, H. Frahm, F. Göhmann, A. Klümper, and V. E. Korepin, *The One-Dimensional Hubbard Model*, (Cambridge University Press, 2005).
- [43] F. Gebhard, *The Mott Metal-Insulator Transition*, (Springer Berlin Heidelberg, Berlin, Heidelberg, 1997).
- [44] T. Giamarchi, *Quantum Physics in One Dimension*, (Oxford University Press, 2003).
- [45] A. Osterkorn, C. Meyer, and S. R. Manmana, In-gap band formation in a periodically driven charge density wave insulator, *Commun. Phys.* **6**, 245 (2023).
- [46] K. Zawadzki and A. E. Feiguin, Time- and momentum-resolved tunneling spectroscopy of pump-driven nonthermal excitations in Mott insulators, *Phys. Rev. B* **100**, 195124 (2019).
- [47] W. H. Press, S. A. Teukolsky, W. T. Vetterling, and B. P. Flannery, *Numerical Recipes in C++*, 2nd ed., (Cambridge University Press, 1993).
- [48] M. H. Kalthoff, G. S. Uhrig, and J. K. Freericks, Emergence of Floquet behavior for lattice fermions driven by light pulses, *Phys. Rev. B* **98**, 035138 (2018).
- [49] G. S. Uhrig, M. H. Kalthoff, and J. K. Freericks, Positivity of the Spectral Densities of Retarded Floquet Green Functions, *Phys. Rev. Lett.* **122**, 130604 (2019).
- [50] C. Meyer, *Matrix Product State Approaches to Non-equilibrium Spectral Quantities of Strongly Correlated Fermions in One Dimension*, Ph.D. thesis, Göttingen University (2022).
- [51] S. R. White, Density matrix formulation for quantum renormalization groups, *Phys. Rev. Lett.* **69**, 2863 (1992).
- [52] S. R. White, Density-matrix algorithms for quantum renormalization groups, *Phys. Rev. B* **48**, 10345 (1993).
- [53] I. P. McCulloch, From density-matrix renormalization group to matrix product states, *Journal of Statistical Mechanics: Theory and*

- Experiment **2007**, P10014 (2007).
- [54] U. Schollwöck, The density-matrix renormalization group in the age of matrix product states, *Annals of Physics* **326**, 96 (2011), january 2011 Special Issue.
- [55] S. Paeckel and T. Köhler, SymMPS toolkit, <https://www.symmps.eu/>, [Online; accessed 13-10-2021].
- [56] E. H. Lieb and F. Y. Wu, Absence of Mott Transition in an Exact Solution of the Short-Range, One-Band Model in One Dimension, *Phys. Rev. Lett.* **21**, 192 (1968).
- [57] J. Haegeman, C. Lubich, I. Oseledets, B. Vandereycken, and F. Verstraete, Unifying time evolution and optimization with matrix product states, *Phys. Rev. B* **94**, 165116 (2016).
- [58] S. Paeckel, T. Köhler, A. Swoboda, S. R. Manmana, U. Schollwöck, and C. Hubig, Time-evolution methods for matrix-product states, *Annals of Physics* **411**, 167998 (2019).
- [59] M. P. Zaletel, R. S. K. Mong, C. Karrasch, J. E. Moore, and F. Pollmann, Time-evolving a matrix product state with long-ranged interactions, *Phys. Rev. B* **91**, 165112 (2015).
- [60] A. Alvermann and H. Fehske, High-order commutator-free exponential time-propagation of driven quantum systems, *Journal of Computational Physics* **230**, 5930 (2011).
- [61] E. M. Stoudenmire and S. R. White, Minimally entangled typical thermal state algorithms, *New Journal of Physics* **12**, 055026 (2010).
- [62] K. Liang, L. Bi, Q. Zhu, H. Zhou, and S. Li, Ultrafast Dynamics Revealed with Time-Resolved Scanning Tunneling Microscopy: A Review, *ACS Applied Optical Materials* **1**, 924 (2023).
- [63] T. Esslinger, Fermi-Hubbard Physics with Atoms in an Optical Lattice, *Annual Review of Condensed Matter Physics* **1**, 129 (2010).
- [64] W. S. Bakr, J. I. Gillen, A. Peng, S. Fölling, and M. Greiner, A quantum gas microscope for detecting single atoms in a Hubbard-regime optical lattice, *Nature* **462**, 74 (2009).
- [65] E. Haller, J. Hudson, A. Kelly, D. A. Cotta, B. Peaudecerf, G. D. Bruce, and S. Kuhr, Single-atom imaging of fermions in a quantum-gas microscope, *Nature Physics* **11**, 738 (2015).
- [66] A. Bohrdt, D. Greif, E. Demler, M. Knap, and F. Grusdt, Angle-resolved photoemission spectroscopy with quantum gas microscopes, *Phys. Rev. B* **97**, 125117 (2018).
- [67] P. T. Brown, E. Guardado-Sanchez, B. M. Spar, E. W. Huang, T. P. Devereaux, and W. S. Bakr, Angle-resolved photoemission spectroscopy of a Fermi-Hubbard system, *Nature Physics* **16**, 26 (2020).